

1       **Generation and characterisation of two D2A1 mammary cancer sublines to**  
2       **model spontaneous and experimental metastasis in a syngeneic BALB/c host**

3  
4       <sup>1,5</sup>Ute Jungwirth, <sup>1</sup>Antoinette van Weverwijk, <sup>1,2</sup>Miriam J. Melake, <sup>3</sup>Ann F. Chambers,  
5                                   <sup>1</sup>Qiong Gao, <sup>1,4</sup>Marc Fivaz and <sup>1,5</sup>Clare M. Isacke

6  
7  
8       <sup>1</sup>The Breast Cancer Now Toby Robins Research Centre, The Institute of Cancer  
9       Research, 237 Fulham Road, London SW3 6JB, UK

10  
11       <sup>2</sup>German Cancer Research Center, DKFZ, Heidelberg, Germany

12  
13       <sup>3</sup>University of Western Ontario, London, Ontario, Canada

14  
15       <sup>4</sup>Current address. Faculty of Engineering & Science, University of Greenwich at  
16       Medway, Kent, ME4 4TB

17  
18  
19       <sup>5</sup>Correspondence to Ute Jungwirth (ute.jungwirth@icr.ac.uk) or Clare M. Isacke  
20       (clare.isacke@icr.ac.uk)

21  
22       **Running Title:** Metastatic mammary cancer model

23  
24  
25       **Keywords:** mammary cancer, metastatic sublines, syngeneic, spontaneous  
26       metastasis, D2A1, BALB/c

27  
28       **Summary statement:** We describe two D2A1 mouse mammary cancer sublines with  
29       enhanced spontaneous metastasis in a syngeneic host, and highlight the limitations  
30       of *in vitro* assays to predict *in vivo* metastatic behaviour.

1 **Abstract**

2

3 Studying the complex mechanisms underlying breast cancer metastasis and therapy  
4 response necessitates relevant *in vivo* models, particularly syngeneic models with an  
5 intact immune system. Two syngeneic spontaneously metastatic sublines, D2A1-m1  
6 and D2A1-m2, were generated from the poorly metastasising BALB/c-derived D2A1  
7 cell line by serial *in vivo* passaging. *In vivo* and *in vitro* analyses revealed distinct and  
8 shared characteristics of the metastatic D2A1-m1 and D2A1-m2 sublines. In  
9 particular, D2A1-m1 cells are more aggressive in experimental metastasis assays,  
10 while D2A1-m2 cells are more efficient at disseminating from the primary tumour in  
11 spontaneous metastasis assays. Surprisingly, classical metastasis-associated *in vitro*  
12 phenotypes such as enhanced proliferation, migration and invasion are reduced in  
13 the sublines compared to the parental cell line. Further, evasion of immune control  
14 cannot fully explain their enhanced metastatic properties. By contrast, both sublines  
15 show increased resistance to apoptosis when cultured in non-adherent conditions  
16 and, for the D2A1-m2 subline, increased 3D tumour spheroid growth. Moreover, the  
17 enhanced spontaneous metastatic phenotype of the D2A1-m2 subline is associated  
18 with an increased ability to recruit an activated tumour stroma. The metastatic D2A1-  
19 m1 and D2A1-m2 cell lines provide additional syngeneic models for investigating the  
20 different steps of the metastatic cascade and thereby represent valuable tools for  
21 breast cancer researchers. Finally, this study highlights that morphology and cell  
22 behaviour in 2D cell-based assays cannot be used as a reliable predictor of  
23 metastatic behaviour *in vivo*.

24

25

26 **Introduction**

27 To study the complex mechanisms of breast cancer metastasis and therapy  
28 response in advanced disease, it is important to have relevant *in vivo* models. Ideally,  
29 the model recapitulates the full metastatic cascade including growth of a primary  
30 tumour, dissemination of tumour cells into the circulation, colonisation of secondary  
31 sites and the development of macrometastatic disease. In addition, to assess the  
32 impact of the immune system, an immunocompetent syngeneic model is required. A  
33 recent study has molecularly characterised 12 mouse mammary cancer cell lines and  
34 performed phenotypic analysis of the primary tumours grown in syngeneic hosts  
35 (Yang et al., 2017). To date, the best characterised spontaneous breast cancer  
36 metastasis model is the BALB/c-derived 4T1 cell line (Aslakson and Miller, 1992) and  
37 the 4T1 sublines selected for increased metastasis to the bone and lung (Lelekakis et

1 al., 1999; Tester et al., 2000) or brain (Lockman et al., 2010). More recently  
2 Johnstone and colleagues have derived and characterised a spontaneously  
3 metastasising variant of the C57BL/6-derived murine medullary mammary  
4 adenocarcinoma cell line E0771 (Johnstone et al., 2015), allowing for metastasis  
5 studies to be performed in an alternative mouse strain. However, there is still an  
6 increasing demand for independent models both for study validation and to address  
7 the inter- and intra-tumour heterogeneity of human disease.

8 In this study we describe the generation of two breast cancer cell sublines,  
9 D2A1-m1 and D2A1-m2, derived from parental D2A1 cells. The parental D2A1 cell  
10 line was derived from a mouse mammary tumour in a BALB/c mouse implanted with  
11 the transplantable D2 hyperplastic alveolar nodule cell line (Mahoney et al., 1985;  
12 Miller et al., 1989; Morris et al., 1993). In a recent comprehensive analysis of 12  
13 mouse mammary cancer cell lines (Yang et al., 2017), D2A1 cells are classified as  
14 oestrogen receptor (ER) and ErbB2/HER2-negative, *Pik3ca* and *Trp53* wildtype,  
15 having a 'claudin-low' transcriptional profile and assignment to the luminal B subtype.  
16 *In vivo*, D2A1 tumours have a spindle-cell histology with ~18% Ki67-positive cells  
17 and ~20% caspase 3-positive nuclei. It was originally reported that 4 weeks after  
18 orthotopic inoculation into immunocompromised nude BALB/c mice, 2 out of the 5  
19 mice showed visible macrometastatic disease in the lungs with the remaining mice  
20 showing lung micrometastatic disease upon histological examination (Morris et al.,  
21 1993). Subsequently it was reported that parental D2A1 cells can colonise the lungs  
22 of immunocompetent BALB/c mice if injected via the tail vein in an experimental  
23 metastasis assays (Shibue and Weinberg, 2009) and that rates of spontaneous  
24 metastasis in BALB/c can be increased by pre-irradiation of the mammary gland  
25 (Bouchard et al., 2013), albeit still with a relatively low metastatic burden.

26 The D2A1-m1 and D2A1-m2 sublines were derived by serial inoculation of  
27 tumour cells in BALB/c mice followed by recovery from the lung tissue *ex vivo*.  
28 Characterisation of these two metastatic sublines demonstrates them to have both  
29 overlapping and distinct phenotypes in *in vivo* assays, *in vitro* assays and by gene  
30 expression profiling. In particular, the D2A1-m1 subline displays an enhanced ability  
31 to colonise the lungs and other tissues in experimental metastasis assays whereas  
32 the D2A1-m2 subline shows a robust and reproducible ability to colonise the lungs in  
33 a spontaneously metastasis assay (inoculation into the mammary fat pad),  
34 associated with an increased ability to recruit an activated tumour stroma.  
35 Consequently, these two D2A1 sublines provide useful and complementary models  
36 to interrogate the different stages of the metastatic cascade.

37

1

## 2 **Results**

### 3 Generation of spontaneously metastatic D2A1 sublines

4 The scheme for the generation of the D2A1 sublines is shown in Fig. 1A. The two  
5 sublines were derived independently. In brief, for each subline, parental D2A1 cells  
6 were inoculated orthotopically into the 4th mammary fat pad of an immunocompetent  
7 BALB/c mouse. When the primary tumour reached 10 - 12 mm in diameter, the lungs  
8 were harvested individually from each mouse at necropsy, dissociated, and placed  
9 into culture. Tumour cells that grew out were expanded and inoculated into the tail  
10 vein of a recipient mouse and 11 - 13 days later, lungs removed at necropsy. In total,  
11 three rounds of intravenous inoculation were performed resulting in the selection of  
12 the independent metastatic sublines, D2A1-m1 and D2A1-m2.

13 In an initial experiment to assess the metastatic competency of the selected  
14 sublines, parental D2A1, D2A1-m1 and D2A1-m2 cells were inoculated orthotopically  
15 into the mammary fat pad of recipient BALB/c mice. Animals were culled individually  
16 between days 31 and 39 when the primary tumours reached 12 - 14 mm in diameter  
17 (Fig. 1B). Consistent with the published literature (Bouchard et al., 2013; Morris et al.,  
18 1993; Yang et al., 2017) parental D2A1 cells readily formed primary tumours but, with  
19 the exception of a single large metastatic nodule in one mouse, gave rise to only  
20 small metastatic nodules in the lungs and with the majority of mice having  
21 undetectable metastatic disease. All mice inoculated with D2A1-m1 and D2A1-m2  
22 cells had metastatic disease as monitored both by tumour area and number of  
23 metastatic nodules, with the D2A1-m2 subline giving rise to the highest metastatic  
24 burden in this spontaneous metastasis assay. Though there is a difference in the  
25 number of metastatic nodules in mice inoculated with the D2A1-m1 and D2A1-m2  
26 sublines and an increase in the % tumour area in the lungs, the average size of the  
27 lung nodules is similar. Of note, although the D2A1-m1 and D2A1-m2 primary  
28 tumours grew slightly faster than the parental D2A1 tumours, in subsequent  
29 experiments no differences in primary tumour growth was observed (see below).

30 To better mimic the clinical setting in breast cancer, spontaneous metastasis  
31 assays in BALB/c mice were then performed in which the primary tumour was  
32 surgically resected at a small size (~ 6 mm in diameter; day 11 - 13) and all mice  
33 were culled on day 43 (Fig. 1C). Despite the increased length of time of the  
34 experiment, when lungs were examined at autopsy, there was only limited metastatic  
35 disease in the parental D2A1 inoculated mice whereas the D2A1-m2 subline gave  
36 rise to extensive tumour burden in the lungs. The D2A1-m1 subline gave mixed  
37 results with 2 out of 5 mice showing no metastatic disease and the remaining 3 mice

1 having readily detectable macrometastatic nodules. The enhanced metastatic burden  
2 observed in mice where the primary tumour is resected (Fig. 1C) likely reflects two  
3 factors. First, in experiments where the primary tumour was not removed, mice were  
4 culled when the primary tumour reached its maximum allowable size (31 - 39 days  
5 (Fig. 1B). By contrast, following tumour resection the study was conducted over a  
6 longer time period (43 days) allowing increased growth of metastatic deposits  
7 (Francia et al., 2011). Second, in experimental mouse models, there have been  
8 numerous reports that removal of a primary tumour can enhance growth of  
9 metastatic lesions (O'Reilly et al., 1994). In addition, these observations suggest that  
10 dissemination of cells from the primary tumour is an early event.

11 To assess whether the immune system plays a role in limiting D2A1 tumour  
12 growth and metastasis, parental D2A1 cells and the metastatic D2A1-m2 subline  
13 were inoculated orthotopically into immunocompetent BALB/c (Supplementary Figure  
14 S1) or immunocompromised NOD scid gamma (NSG) (Fig. 2) mice. In both mouse  
15 strains, there was no significant difference in primary tumour growth but, again, the  
16 D2A1-m2 cells gave rise to a significantly increased metastatic burden in the lung.  
17 Moreover, although the primary tumours did not grow at a noticeably faster rate in the  
18 NSG compared to the BALB/c mice (Fig. 2A, Supplementary Figure S1A), it is  
19 important to note that the NSG mice experiment had to be terminated at an earlier  
20 time (and when the primary tumours were of a much smaller size) due to the  
21 extensive burden of metastatic disease in the D2A1-m2 inoculated mice (Fig. 2B). In  
22 addition, although the D2A1 parental cells showed a much reduced metastatic  
23 burden compared to the D2A1-m2 subline, the amount of D2A1 metastatic burden in  
24 the lung was greater in the immunocompromised NSG mice compared to the BALB/c  
25 mice. Although, differences in tumour growth can vary between different mouse  
26 strains (Hunter, 2006) these data suggest that both the D2A1 parental cells and their  
27 metastatic derivatives are under immune control, particularly in the metastatic setting,  
28 and that evasion of immune control cannot fully explain the enhanced metastatic  
29 properties of the metastatic subline.

30

### 31 Experimental metastasis assays

32 Next we assessed the ability of the two metastatic sublines to colonise secondary  
33 sites in different experimental metastasis assays. First, untagged (Fig. 3A) or  
34 luciferase tagged (Supplementary Figure S2) tumour cells were inoculated  
35 intravenously into recipient BALB/c mice. Consistent with the spontaneous  
36 metastasis assays, injection of both sublines resulted in a greater lung tumour  
37 burden than the parental cells. Interestingly, although the D2A1-m2 subline gave rise

1 to a higher burden of spontaneous lung metastases compared to the D2A1-m1  
2 subline (Fig. 1B), in this experimental metastasis assay it was the D2A1-m1 subline  
3 that gave rise to the greatest lung tumour burden (Fig. 3A).

4 Intravenous inoculation results in the majority of tumour cells lodging in the  
5 lungs. To investigate other sites of metastasis, we next performed intracardiac  
6 inoculation of tumour cells (Fig. 3B), which favours dissemination via the arterial  
7 system to the bones, brain and other organs (Bos et al., 2009; Khanna and Hunter,  
8 2005). *Ex vivo* IVIS imaging revealed that, again, the D2A1-m1 subline gave rise to  
9 the greatest tumour burden in the bones. Neither the D2A1 parental cells nor the  
10 metastatic sublines showed evidence of brain colonisation.

11 Finally, we performed intrasplenic inoculations to assess colonisation of the  
12 liver (Khanna and Hunter, 2005) (Fig. 3C). 50% of mice inoculated with parental  
13 D2A1 cells had undetectable tumour burden in the liver but both the D2A1-m1 and  
14 D2A1-m2 sublines gave rise to extensive disease with only one mouse in each group  
15 remaining tumour free.

16 Together these *in vivo* experiments, indicate that the two D2A1 sublines have  
17 different properties with the D2A1-m1 subline having a superior ability to grow in the  
18 lungs and the bones but, compared to the D2A1-m2 subline, a reduced ability to  
19 disseminate from the primary tumour. Consequently, we next addressed whether  
20 these two sublines displayed altered properties using a panel of *in vitro* proliferation,  
21 migration and invasion assays.

#### 22 D2A1 metastatic sublines in adherent culture.

24 When growing as adherent cultures on tissue culture plastic the D2A1 metastatic  
25 sublines have distinct morphologies, with D2A1-m1 cells having a more elongated  
26 shape and D2A1-m2 cells being more rounded, compared to the parental cells (Fig.  
27 4A; Supplementary Fig. S3). These different morphologies did not impact on the  
28 plating efficiency as exemplified by all three cell lines giving rise to the same number  
29 of colonies in a colony formation assay (Fig. 4B). By contrast, in this assay, it was  
30 notable that the two metastatic sublines gave rise to smaller colonies, indicating a  
31 lower proliferation rate *in vitro*. Consistent with this, both sublines displayed a lower  
32 proliferation rate as continuously monitored in the IncuCyte live cell analysis (Fig. 4C)  
33 and reduced cell number over time as monitored in the CellTiter-Glo assay (Fig. 4D).  
34 Together with the observation that there was no consistent difference in primary  
35 tumour growth between the parental line and the sublines, these data indicate that  
36 the increased metastatic ability of the sublines is not due to the acquisition of a more  
37 proliferative phenotype.

1 Next we tested whether the sublines show a difference in their migratory  
2 abilities, a characteristic linked to an increased metastatic potential. To our surprise,  
3 both sublines displayed a reduced migratory and chemotactic capacity *in vitro* as  
4 monitored in the IncuCyte scratch wound assay (Fig. 4E) and a Transwell  
5 chemotactic assay (Fig. 4F). These data highlight how morphology and cell  
6 behaviour in 2D adherent assays cannot be used as a predictor of metastatic  
7 behaviour *in vivo*. Consequently we moved to assays under non-adherent conditions.

#### 8 9 D2A1 metastatic sublines in non-adherent culture.

10 As an example of how non-adherent assays can reveal properties of cells that are  
11 not evident in adherent assays, D2A1 parental cells and the D2A1 metastatic  
12 sublines D2A1 were seeded into tissue culture or low adherence plates and  
13 monitored for apoptosis after 24 hours (Fig. 5A). In adherent culture, essentially all  
14 cells were viable as monitored by the lack of annexin V (AV) staining and propidium  
15 iodide (PI) uptake. After 24 hours in non-adherent culture more than 50% of the  
16 D2A1 parental cells were classed as early apoptotic (AV+/PI-), late apoptotic  
17 (AV+/PI+) or necrotic (AV-/PI+), while both the D2A1-m1 and D2A1-m2 sublines  
18 showed a significantly lower level of anoikis under these conditions. To explore this  
19 further, we next plated cells into low-adherence U bottom plates (Fig. 5B). The  
20 parental cells readily assembled into dense tumour spheroids with well delineated  
21 margins, and expanded in size over time. Of the two metastatic sublines, the D2A1-  
22 m1 subline again assembled into tumour spheroids but, consistently, they were less  
23 regular in shape. However, there was no difference in D2A1-m1 spheroid growth  
24 compared to the parental cells. By contrast, the D2A1-m2 subline formed less well  
25 aggregated spheroids with loosely attached cells associated with the main core.  
26 Moreover, as monitored by CellTiter-Glo, these disorganised spheroids showed a  
27 significant increase in cell number over time compared to the parental D2A1 and  
28 D2A1-m1 spheroids.

29 Given the less regular spheroid shape formed by the D2A1 sublines, we  
30 anticipated that the more loosely attached tumour cells might be more invasive. To  
31 address this, tumour spheroids were transferred after 3 days into a collagen matrix.  
32 At the indicated time points, collagen plugs were fixed, stained with DAPI and cell  
33 invasion into the 3D collagen matrix quantified. Surprisingly, the parental D2A1 cells  
34 were significantly more invasive than either of the metastatic sublines. Despite the  
35 limitation of using *in vitro* assays to model *in vivo* metastasis, these data point to the  
36 metastatic sublines having an enhanced metastatic capacity due to their ability to  
37 resist stress-induced anoikis.

1  
2  
3  
4  
5  
6  
7  
8  
9  
10  
11  
12  
13  
14  
15  
16  
17  
18  
19  
20  
21  
22  
23  
24  
25  
26  
27  
28  
29  
30  
31  
32  
33  
34  
35  
36  
37

## D2A1-m2 cells promote stromal cell activation

To investigate further how these differing behaviours in non-adherent culture might impact on tumour growth *in vivo*, primary tumours in BALB/c mice (Fig. 1B, Supplementary Figure S1A) and NSG mice (Fig. 1C) were sectioned and stained for  $\alpha$ SMA, a marker of activated fibroblasts and endomucin, a marker of endothelial cells. The elevated levels of  $\alpha$ SMA-positive fibroblasts and blood vessels in the D2A1-m2 primary tumours in both the BALB/c immunocompetent (Fig. 6A, Supplementary Figure S1D,E) and NSG immunocompromised (Fig. 6B) mice suggest that this subline has an enhanced ability to promote stromal cell recruitment activation and this may, in part, provide a mechanistic explanation for the enhanced spontaneous dissemination of tumour cells to secondary sites.

Although stromal cell activation and recruitment observed in *in vivo* tumours cannot be fully recapitulated *in vitro*, we examined whether the metastatic sublines had an increased ability to promote directional migration of fibroblasts using the 'ibidi'  $\mu$ -slide chemotaxis system. 3T3 mouse fibroblasts were plated into the central viewing chamber that is connected to two larger reservoirs on either side (Supplementary Figure S4A). By plating different cell populations into the two reservoirs, conditioned medium gradients are set up and cell migration can be monitored by time-lapse microscopy. As expected, if D2A1 cells are plated into both reservoirs, there is no bias in the directional migration of the fibroblasts (Fig. 6C; left panel). However, if D2A1 cells are plated into one reservoir and either D2A1-m1 or D2A1-m2 cells are plated into the other, the fibroblasts show preferential displacement towards the metastatic sublines over the parental cells (see Supplementary Figure S4B for individual fibroblast migration tracks). However, albeit with relatively small effects, only the D2A1-m2 subline induced a significant difference in fibroblast migration speed (velocity) and Euclidean distance migrated (Fig. 6C; middle and right panels) and a significant fibroblast chemotaxis (Rayleigh test; Supplementary Figure S4C). Finally, to assess the capacity of the metastatic sublines to promote fibroblast activation, fibroblasts were embedded into a Matrigel/collagen gel and treated with conditioned media from D2A1, D2A1-m1 or D2A1-m2 cells or with TGF $\beta$  as a positive control (Fig. 6D). Only D2A1-m2 conditioned medium and TGF $\beta$  treatment resulted in a significant induction of fibroblast contractility. Consistent with the *in vivo* observations (Fig. 6A) these data indicate that the D2A1-m2 subline has an enhanced ability to both recruit and activate stromal fibroblasts.



1 Gene expression profiling and analysis of human datasets

2 Finally, we subjected the parental D2A1 cells and metastatic sublines to gene  
3 expression profiling. Principle component analysis revealed that each cell line was  
4 qualitatively unique, with the metastatic sublines being distinct but more closely  
5 related to each other than to the parental cells (Fig. 7A). Overall, there were 890  
6 genes differentially expressed between the D2A1-m1 cells and parental D2A1 cells,  
7 from which 323 genes were with a fold change of  $\geq 1.5$ -fold. In the case of the D2A1-  
8 m2 cells, 1339 genes were differentially expressed, from which 318 had a fold  
9 change  $\geq 1.5$  (Fig 7B). A comparison of the differentially expressed genes showed  
10 that approximately 50% were unique to each subline and 50% overlapped as shown  
11 in the Venn diagram (Fig 7B bottom panel). Unsupervised two-dimensional  
12 hierarchical clustering of the D2A1, D2A1-m1 and D2A1-m2 cells (based on genes  
13 with a fold change  $\geq 1.5$ , using their log<sub>2</sub> gene expression) confirmed the close  
14 relationship of the two sublines but also distinct gene expression patterns (Fig 7C).  
15 Top differentially expressed genes for D2A1-m1 vs. D2A1 and D2A1-m2 vs. D2A1  
16 are shown in Supplementary Table S1 and Supplementary Table S2, respectively.  
17 Top genes that were differentially changed in both sublines (Fig. 7B) and their  
18 average fold change are shown in Supplementary Table S3. Similarly, Ingenuity  
19 Pathway Analysis demonstrated distinct top canonical pathways, while the upstream  
20 regulators and molecular and cellular functions were highly overlapping (Fig. 7D,  
21 Supplementary Tables S4 and S5). Even though in both, D2A1-m1 and D2A1-m2  
22 cells, TGF $\beta$ 1 is identified as upstream regulator, only in D2A1-m2 subline is the  
23 predictive z-score  $> 2$  fold, indicating a stronger activation of this pathway in D2A1-m2  
24 cells than in the parental and D2A1-m1 cells, and potentially accounting for the  
25 observed ability of the D2A1-m2 subline to promote stromal activation.

26

27 **Discussion**

28 Studying the complex mechanisms driving breast cancer metastasis and therapeutic  
29 response of advanced disease has been hampered by the lack of robust *in vivo*  
30 models, and in particular spontaneously metastatic syngeneic models where the  
31 interaction with an intact immune system can be studied. To date, there has been  
32 heavy reliance on the BALB/c-derived 4T1 cell line (Aslakson and Miller, 1992;  
33 Fantozzi and Christofori, 2006) as 4T1 cells, and selected 4T1 sublines, readily form  
34 primary orthotopic tumours that can spontaneously metastasise to the lungs and  
35 other secondary sites (Eckhardt et al., 2005; Fantozzi and Christofori, 2006; Yang et  
36 al., 2004). More recently Johnstone and colleagues have described the generation of  
37 a spontaneously metastatic E0771.LMB subline from the C57BL/6-derived E0771

1 mouse medullary mammary adenocarcinoma E0771 cell line (Johnstone et al., 2015)  
2 that provides a valuable model in a different mouse strain (Chen et al., 2017). The  
3 molecular and phenotypic characterisation of 12 mouse mammary carcinoma cell  
4 lines (Yang et al., 2017), provides valuable information for the research community  
5 but, as the authors note, the efficiency of metastatic spread with these lines lacks  
6 reproducibility, for example only 45% of the mice inoculated with parental D2A1 cells  
7 had detectable metastatic lesions in the lungs. Alternatives to syngeneic mouse cell  
8 lines are tumour prone genetically modified mice (Fantozzi and Christofori, 2006)  
9 such as those expressing a polyoma middle T (PyMT) (Guy et al., 1992a) or  
10 ErbB2/neu (Guy et al., 1992b) transgene in the mammary gland. Genetically modified  
11 models have provided powerful insights into tumour initiation and progression, but  
12 they have limitations when studying the development of distant metastases due to  
13 the variable latency and often late presentation of secondary disease, and the  
14 inability to rapidly perform additional genetic manipulation. In addition to the mouse  
15 syngeneic models, there are many human breast cancer cell lines that can be grown  
16 as xenografts in immunocompromised mice, and more recently, an increasing  
17 number of patient-derived xenografts where primary tumour material is transplanted  
18 directly into immunocompromised mice and then serially passaged. Such models  
19 have been extremely valuable in studying the heterogeneity of human disease and  
20 for monitoring response to tumour targeting agents (Bruna et al., 2016; Byrne et al.,  
21 2017; Holen et al., 2017; Neve et al., 2006). However, few of these models  
22 reproducibly spontaneously metastasise. Further, the lack of a species matched  
23 stroma and the lack of an intact immune system limit the interrogation of breast  
24 cancer biology and/or the assessment of stromal targeting agents. Consequently,  
25 there remains an urgent need to develop a wider variety of syngeneic models where  
26 the different stages of the metastatic cascade can be investigated.

27         In this study we describe the generation and characterisation of two sublines  
28 of the poorly metastatic mouse mammary tumour cell line, D2A1. These sublines,  
29 D2A1-m1 and D2A1-m2, reproducibly give rise to spontaneous metastases from the  
30 primary tumour to the lungs, and in experimental metastasis assays readily colonise  
31 the lung, liver, and in case of the D2A1-m1 subline, bone. However, there are notable  
32 differences in the behaviour of these two sublines *in vivo*. In particular, the D2A1-m1  
33 subline, compared to the D2A1-m2 subline, is less efficient at disseminating from the  
34 primary tumour in a spontaneous metastasis assay but more efficient at colonising  
35 the lungs, bone and liver when inoculated via the tail vein, the left ventricle of the  
36 heart or the spleen, respectively. This would suggest that the D2A1-m1 subline has  
37 acquired properties that better enable it to extravasate from the circulation and/or

1 efficiently proliferate at these secondary sites and that, conversely, the D2A1-m2 has  
2 acquired properties that better enable it to disseminate from the primary tumours.

3 To address the potential mechanism underlying these distinct phenotypes,  
4 first we extensively characterised these cells lines in *in vitro* assays. In adherent  
5 cultures, the two sublines have distinct morphologies with the D2A1-m1 cells having  
6 a more elongated and the D2A1-m2 cells have a more rounded shape. However,  
7 these morphological differences did not relate to their behaviour with both sublines,  
8 surprisingly, showing a lower rate of proliferation and migration compared to the  
9 parental D2A1 cells. More revealing was their behaviour in non-adherent conditions.  
10 When normal epithelial cells are detached from a matrix, a programme of caspase-  
11 mediated apoptosis, known as anoikis, is activated (Frisch and Screaton, 2001; Paoli  
12 et al., 2013). A hallmark of cancer is 'resisting cell death' (Hanahan and Weinberg,  
13 2011) and D2A1 parental cells show evidence of such resistance as evidenced by  
14 their ability to form and proliferate as free floating tumour spheroids when plated into  
15 U bottom low attachment plates. However, when plated under conditions that do not  
16 promote cell:cell contact between the detached cells (low adherent flat bottom plates)  
17 within 24 hours over 50% of the D2A1 cells show markers of apoptotic cell death,  
18 compared to <10% of the cells plated onto adherent flat bottomed plates. In the same  
19 assays, both metastatic sublines show increased resistance to anoikis, and in  
20 spheroid culture the D2A1-m2 cells show enhanced proliferative ability.

21 Consequently, we conclude that the increased metastatic potential of the two  
22 sublines is due, at least in part, to their ability to survive in a more hostile  
23 environment. However, these *in vitro* studies were relatively uninformative as to why  
24 the D2A1-m1 subline shows a more aggressive behaviour in experimental metastasis  
25 assays. Some clues are provided by gene expression profiling where examination of  
26 genes differentially expressed between the D2A1-m1 subline and the parental cells  
27 revealed that upregulation of canonical pathways involved in glutathione regulation  
28 and the actin cytoskeleton, features that may provide an advantage for the cells in  
29 extravasating from the circulation and/or surviving in the foreign metastatic  
30 environments. Future studies will be required to fully address this hypothesis and it  
31 will certainly be of interest to compare the transcriptional profile of the D2A1 sublines  
32 freshly isolated from tumours, as this may well be more informative than profiling the  
33 sublines grown in culture.

34 More informative was the analysis of the D2A1-m2 subline. In addition to  
35 showing an increased resistance to anoikis, the D2A1-m2 primary tumours, in both  
36 immunocompetent BALB/c mice and immunocompromised NSG mice, showed  
37 striking infiltration of  $\alpha$ SMA-positive stromal fibroblasts and pericytes. At least in part,

1 this phenotype could be recapitulated *in vitro* where we show that when presented  
2 with an option for directional migration, cultured fibroblasts preferentially migrate, at  
3 an increased velocity, towards the D2A1-m2 subline and D2A1-m2 conditioned  
4 medium, but not conditioned medium from D2A1 or D2A1-m1 cells, promoted  
5 fibroblast activation as monitored in a gel contraction assay. A number of studies  
6 have demonstrated that an activated stroma, in particular the presence of activated  
7 pericytes on the blood vessels, is required for efficient intravasation of tumour cells  
8 from the primary tumour into the circulation (Harney et al., 2015; Viski et al., 2016;  
9 Xian et al., 2006; Yang et al., 2016) and an activated cancer-associated fibroblasts  
10 can prime tumour cells for metastatic growth (Zhang et al., 2013). The data  
11 presented here suggest that the increased efficiency of the D2A1-m2 subline to  
12 spontaneously metastasise may, at least in part, result from the ability to recruit and  
13 activate stromal cells, particularly stromal fibroblasts and pericytes.

14 In summary, the data presented here describes the derivation and  
15 characterisation of two new syngeneic metastatic mouse mammary carcinoma cell  
16 lines that have both overlapping and distinct behaviours when introduced into mice.  
17 Surprisingly, the ability of these cells to give rise to both spontaneous and  
18 experimental metastases *in vivo*, is not reflected by a more aggressive phenotype in  
19 *in vitro* proliferation, migration and invasion assays. However, some clues as to the  
20 mechanisms driving the metastatic phenotype have been revealed by assessing the  
21 cell lines in non-adherent culture and by examination of the tumour stroma.

22  
23  
24

## 25 **Methods**

### 26 *In vivo* studies

27 All *in vivo* studies were performed under UK Home Office Project Licenses 70/7413  
28 and P6AB1448A granted under the Animals (Scientific Procedures) Act 1986. All  
29 studies were performed at The Institute of Cancer Research (Establishment Licence,  
30 X702B0E74 70/2902). Ethical permission was granted by the Institute of Cancer  
31 Research "Animal Welfare and Ethical Review Body" (AWERB). Female BALB/c and  
32 NSG mice (Charles River) between 6 and 12 weeks of age were housed in  
33 individually ventilated cages, monitored on a daily basis for signs of ill health and had  
34 food and water ad libitum. In all cases, experiments were terminated if the primary  
35 tumour reached a maximum allowable diameter of 15 mm or if a mouse showed  
36 signs of ill health.

1           The two metastatic sublines were generated independently (see Fig. 1A). In  
2 each case,  $5 \times 10^4$  D2A1 cells were injected into the 4th mammary fat pad of a single  
3 BALB/c mouse under general anaesthesia. When the primary tumour reached 12 -  
4 14 mm in diameter, lungs were dissected post-mortem, mechanically dissociated and  
5 placed into culture in DMEM (Gibco by ThermoFisher) plus 10% FBS (Gibco by  
6 ThermoFisher) and 1% penicillin/streptomycin. Medium was changed after 24 hours  
7 and then twice a week. After two weeks, when tumour cell colonies were visible, cells  
8 were replated and expanded. Once expanded,  $5 \times 10^4$  cells were injected via the tail  
9 vein into a single BALB/c mouse. After 11-13 days, lungs were processed as before.  
10 The intravenous inoculation was repeated a further 2 times, each time into a single  
11 mouse. This procedure resulted in the two independently selected D2A1 sublines,  
12 D2A1-m1 and D2A1-m2.

13           For spontaneous metastasis assays,  $5 \times 10^4$  cells were injected into the 4th  
14 mammary fat pad of BALB/c or NSG mice under general anaesthesia. Tumour  
15 growth was monitored using callipers and tumour volume calculated as  
16  $0.5236 \times [(width + length)/2]^3$  (Janik et al., 1975). Primary tumours and lung tissue  
17 were formalin-fixed and paraffin-embedded (FFPE) prior to sectioning. FFPE  
18 sections of primary tumours were stained with  $\alpha$ SMA (Sigma, clone 1A4, 1:1000  
19 dilution) or endomucin (Santa Cruz SC-65495; 1:2000 dilution). Detection was  
20 achieved with the VectaStain ABS system and sections were scanned on the  
21 NanoZoomer Digital Pathology (Hamamatsu). HRP staining was analysed in ImageJ  
22 from  $\geq 6$  fields of view per tumour, avoiding areas of necrosis. To quantify lung tumour  
23 burden, sections taken midway through the lung and stained with haematoxylin and  
24 eosin (H&E). Sections were scanned and analysed using the NanoZoomer Digital  
25 Pathology, file names were blinded and the number of macroscopic tumour nodules  
26 (defined as having a minimum area of  $1000 \mu\text{m}^2/\text{nodule}$ ) counted manually or  
27 quantified as % tumour burden. The % lung tumour burden was defined as (total  
28 tumour area)/(lung area)  $\times 100$  from a coronal H&E section of the lung. Where  
29 indicated, primary tumours were surgically resected under general anaesthesia.

30           For intravenous inoculation,  $4 \times 10^5$  cells were injected into the tail vein of  
31 BALB/c mice. After 11 days mice were sacrificed. Lungs were processed as  
32 described in the spontaneous metastasis assay. For intracardiac inoculation,  $2 \times 10^5$   
33 luciferase expressing cells were injected into the left ventricle of BALB/c mice under  
34 general anaesthesia. Tumour burden was analysed by *ex vivo* IVIS imaging. Mice  
35 were injected intraperitoneally with 150 mg/kg D-luciferin (Caliper Life Sciences) in  
36 100  $\mu\text{L}$ . After 5 minutes, dissected hind limb long bones and brains were imaged  
37 using an IVIS imaging chamber (IVIS Illumina II). Luminescence measurements

1 (photons/second/cm<sup>2</sup>) were acquired over 1 minute and analysed using the Living  
2 Image software (PerkinElmer) by placing a constant size region of interest over the  
3 tissues. For intrasplenic inoculation, 2 x 10<sup>5</sup> luciferase expressing cells were  
4 inoculated into the spleen parenchyma of BALB/c mice under general anaesthesia.  
5 After 10 minutes, a splenectomy was performed to avoid growth of splenic tumours.  
6 Tumour burden in the liver was assessed by *ex vivo* IVIS imaging as described  
7 above.

8

### 9 Cell lines

10 D2A1 cells were from Chambers lab stocks, from stocks originally obtained from Dr.  
11 Fred Miller (Mahoney et al., 1985; Miller et al., 1989). NIH-3T3 cell were from Isacke  
12 laboratory stocks. Cells were maintained in DMEM plus 10% FBS and 1%  
13 penicillin/streptomycin. Cells were luciferase transduced with lentiviral expression  
14 particles containing a firefly luciferase gene and a blasticidin-resistance gene  
15 (Amsbio, LVP326). All cells were routinely subject to mycoplasma testing.

16

### 17 *In vitro* studies

18 For cell shape analysis, 1x10<sup>3</sup> cells/well were seeded into a ViewPlate-96 Black with  
19 optically clear bottom (PerkinElmer). After 24 hours, cells were fixed in 4%  
20 paraformaldehyde (PFA), permeabilised with 0.5% Triton X-100 prior to staining with  
21 DAPI (molecular probes, D1306, 1:10,000) and Alexa488-labeled phalloidin  
22 (molecular probes, A12379, 1:500). Automated image acquisition was performed on  
23 an Operetta high content imaging system (Perkin Elmer). Cell shapes were analysed  
24 using basic algorithms in the Harmony high content analysis software package  
25 (Perkin-Elmer). Cells were initially defined using the DAPI channel to identify the  
26 nucleus and the cytoplasm was segmented using the Alexa488 channel. After this,  
27 the Harmony software allows the extraction of cell shape parameters, including “cell  
28 roundness”. On average 1110 cells were analysed per well (n=6 wells/cell line).

29 For cell proliferation/viability assays, 1x10<sup>3</sup> cells/well were seeded into 96-well  
30 plates. Cell viability was quantified either by CellTiter-Glo (Promega) at the indicated  
31 time points or by time-lapse imaging and quantification of cell confluence using the  
32 Live-Cell Analysis System IncuCyte (EssenBioscience).

33 For colony formation assay, 50 cells/well were seeded into a 6-well plate.  
34 Tumour cell colonies were stained 7 days later with crystal violet. Plates were  
35 scanned using the GelCount (Oxford Optronix) and image analysis performed using  
36 GelCount software and ImageJ.

1 For scratch wound migration assays, cells were seeded at high density to  
2 form a confluent layer in a 96 Image Lockplate (EssenBioscience). Scratches were  
3 created using a WoundMaker tool (EssenBioscience). Plates were imaged for 72  
4 hours and analysed using the Live-Cell Analysis System IncuCyte (EssenBioscience).

5 For the Transwell migration assay,  $1 \times 10^3$  cells/well were seeded into  
6 IncuCyte ClearView 96-well chemotaxis plates in DMEM supplemented with 3% FBS.  
7 The bottom well contained DMEM supplemented with 10% FBS. Chemotactic  
8 migration was monitored and analysed using the IncuCyte Chemotaxis System  
9 (EssenBioscience).

10 For competitive fibroblast attraction assays the  $\mu$ -Slide Chemotaxis system  
11 (ibidi) was used. In brief,  $1.2 \times 10^4$  3T3 fibroblasts were seeded into the central  
12 observation chamber. 3 hours later,  $3 \times 10^4$  D2A1 cells were seeded into the left  
13 reservoir and either D2A1, D2A1-m1 or D2A1-m2 cells into the right reservoir.  
14 Migration of 3T3 fibroblasts was imaged over 8 hours (20 minute intervals) using  
15 Slidebook 6 (3i) and a Nikon Eclipse TE2000-5 widefield microscope equipped with a  
16 plan fluor 10x/0.3 ph1 wd 16 objective (Nikon) and a temperature- and CO<sub>2</sub>-  
17 controlled chamber. Cell migration was analysed using the ImageJ Manual tracking  
18 and Chemotaxis and Migration Tool (ibidi) plugin.

19 To collect conditioned media, cells were seeded in DMEM supplemented with  
20 10% FBS and cultured until 70-80% confluency. The media was then changed to  
21 DMEM supplemented with 2% FBS. Conditioned media was collected after 24 hours  
22 and filtered prior to use. For fibroblast contraction assays,  $7 \times 10^4$  3T3 fibroblasts  
23 were embedded in 100  $\mu$ l of a Matrigel (final concentration 2 mg/ml, Corning) and rat  
24 tail Collagen I (final concentration 4 mg/ml, Corning) mixture and seeded onto a glass  
25 bottom dish (P24G-1.0-13-F, MatTek Corporation). After the gel was set at 37°C,  
26 conditioned medium or DMEM supplemented with 2% FBS with or without  
27 recombinant TGF $\beta$ 1 (R&D Systems)(5 ng/ml) was added. After 14 days, plates were  
28 scanned and the contracted gel area was measured using ImageJ.

29 For apoptosis assay,  $5 \times 10^4$  cells/well were plated into either a tissue culture  
30 treated or low adherence 6-well plates. 24 hours after seeding, cells were stained  
31 with the Annexin V-APC/ PI Apoptosis Detection Kit (eBioscience) and analysed  
32 using a BD Biosciences LSRII flow cytometer with FACSDIVA and FlowJo software.

33 For spheroid growth assays,  $1 \times 10^2$  cells were seeded into ultra-low  
34 adherence 96-well round bottom plates (Corning). Spheroid growth was monitored  
35 using the Celigo Image Cytometer (Nexcelom Bioscience). Cell viability was  
36 monitored with CellTiter-Glo at the indicated time points. To ensure proper lysis of

1 the spheroids, the incubation time with the CellTiter-Glo reagent was extended from  
2 10 to 30 minutes before recording luminescence.

3 For invasion assays,  $2 \times 10^4$  cells were seeded into ultra-low adherence 96-  
4 well round bottom plates. 3 days later, spheroids were transferred into fresh round  
5 bottom plates containing 2mg/ml collagen (rat tail collagen, Corning). After 24, 48  
6 and 72 hours collagen plugs were fixed in 4% PFA, permeabilised with 0.5% Triton  
7 X-100 and stained with DAPI. Confocal z-stacks were acquired using the  
8 ImageXpress Micro Confocal High-Content Analysis System (Molecular Devices)  
9 equipped with a 60µm pinhole spinning-disk, and a plan apo  $\lambda$  10x/0.45 objective  
10 (Nikon). z-stacks were maximally projected and DAPI images were quantified using a  
11 custom-written MATLAB script. In brief, spheroids were binarised using an intensity  
12 threshold while individual cells invading into the collagen, away from the spheroid,  
13 were marked using the watershed transform, which allows separation of contacting  
14 cells. The centroid coordinates of the spheroid and individual cells were extracted  
15 and the distance  $d$  between each cell and the spheroid was calculated using  
16 Euclidean trigonometry. The mean square displacement (MSD), a global measure of  
17 invasion, was obtained using the following equation:

$$\text{MSD} = \frac{1}{N} \sum_{k=1}^N d_k^2 \quad (1) \text{ where } d_k \text{ is the distance (in } \mu\text{m)} \text{ between the } k \text{ cell and}$$

18  
19  
20 the spheroid and  $N$  is the total number of cells.

21

## 22 Gene expression profiling and analysis of clinical datasets

23 RNA from D2A1 and D2A1-m2 cultured cells ( $n = 3$  independent biological replicates)  
24 and D2A1-m1 cultured cells ( $n = 2$  independent biological replicates) was extracted  
25 using the RNeasy Mini kit (Qiagen). Microarray experiments were performed in two  
26 independent batches at Cambridge Genomic Services, University of Cambridge. In  
27 brief, RNA was assessed for concentration and quality using a SpectroStar (BMG  
28 Labtech) and a Bioanalyser (Agilent Technologies). The 8 RNA samples were  
29 amplified, labelled and hybridised on a MouseWG-6 v2.0 Expression BeadChip array  
30 (Illumina) following the manufacturer's instructions. Raw expression data were  
31 extracted in R using lumi package (<http://www.bioconductor.org>). Data were filtered  
32 to remove any non-expressed probes (detection  $p > 0.01$ ) across all samples,  
33 transformed using variance-stabilising transformation, normalised using the robust  
34 spline normalisation method, and then batch-corrected using the function (ComBat)  
35 in the R package (sva). Sample relations were estimated using principle component  
36 analysis based on 7970 genes with coefficient of variance (standard deviation/mean  
37  $> 0.1$ ). Two-sample  $t$ -tests were used to identify differentially expressed genes



1 between (a) D2A1 and D2A1-m1, (b) D2A1 and D2A1-m2 and (c) D2A1-m1 and  
2 D2A1-m2, using the BRB-Array Tools (<https://brb.nci.gov/BRB-ArrayTools/>) with a  
3 threshold of parametric  $p$ -value  $< 0.001$ . Differentially expressed genes with a fold  
4 change  $\geq 1.5$  were subject to Ingenuity Pathway Analysis (IPA) to identify altered  
5 pathways, where  $p < 0.05$  were considered as significant. When multiple probes  
6 were mapped to the same gene, the most variable probe measured by interquartile  
7 range (IQR) across the samples was selected to represent the gene. Gene  
8 expression data from this study are deposited at deposited in NCBI Gene Expression  
9 Omnibus (GSE101579).

10

11 Statistics

12 Statistics were performed using GraphPad Prism 6. Unless otherwise stated, all  
13 numerical data are expressed as mean  $\pm$ s.e.m. Significant outliers were identified  
14 using the Grubb's test ( $\alpha = 0.05$ , GraphPad Prism) and are shown as white symbols  
15 in the graphs. If not indicated otherwise, all comparisons between two groups were  
16 made using two-tailed, unpaired Student's  $t$ -test. If there was a significant difference  
17 in the variance of samples a Welch's correction was applied. Where multiple groups  
18 over time were compared, a two-way ANOVA followed by Bonferroni post-hoc testing  
19 was performed. \*,  $p < 0.05$ ; \*\*,  $p < 0.01$ ; \*\*\*,  $p < 0.001$ .

20

21

22 **List of abbreviations**

- 23 a.u., arbitrary units
- 24 AV, annexin V
- 25 cps, counts per second
- 26 DMEM, Dulbecco's Modified Eagle's Medium
- 27 FBS, foetal bovine serum
- 28 IPA, Ingenuity Pathway Analysis
- 29 Luc, luciferase
- 30 MSD, mean square displacement
- 31 NSG, NOD scid gamma
- 32 PFA, paraformaldehyde
- 33 PI, propidium iodide

34

35

36 **Declarations**

37

1 Acknowledgements. We are grateful to the expertise in the Breast Cancer Now  
2 Histopathology Facility and the ICR FACS and Light Microscopy Facility. Cambridge  
3 Genomic Services performed the gene expression analysis. We thank Slavomir  
4 Wantuch for lab support, David Vicente for help with the *in vivo* assays, Fredrik  
5 Wallberg for help with the imaging assays.

6  
7 Competing interests. The authors declare that they have no competing interests

8  
9 Funding. This work was funded by a grant from Worldwide Cancer Research to CMI  
10 and UJ, funding from Breast Cancer Now, working in partnership with Walk the Walk  
11 to CMI. We acknowledge NHS funding to the NIHR Biomedical Research Centre at  
12 The Royal Marsden and the ICR. UJ was a recipient of a Schrödinger fellowship of  
13 the Austrian Science Fund (FWF): J3434-B13. MJM was a recipient of a Helmholtz  
14 International Graduate School for Cancer Research (HIGS) fellowship and part of the  
15 EU-funded ERASMUS Placement Programme.

16  
17 Availability of data and materials. Microarray data have been deposited in NCBI  
18 Gene Expression Omnibus (GSE101579).

19  
20  
21  
22  
23

1 **References**

2 **Aslakson, C. J. and Miller, F. R.** (1992). Selective events in the metastatic  
3 process defined by analysis of the sequential dissemination of subpopulations of a  
4 mouse mammary tumor. *Cancer Res* **52**, 1399-405.

5 **Bos, P. D., Zhang, X. H., Nadal, C., Shu, W., Gomis, R. R., Nguyen, D. X.,**  
6 **Minn, A. J., van de Vijver, M. J., Gerald, W. L., Foekens, J. A. et al.** (2009). Genes  
7 that mediate breast cancer metastasis to the brain. *Nature* **459**, 1005-9.

8 **Bouchard, G., Bouvette, G., Therriault, H., Bujold, R., Saucier, C. and**  
9 **Paquette, B.** (2013). Pre-irradiation of mouse mammary gland stimulates cancer cell  
10 migration and development of lung metastases. *Br J Cancer* **109**, 1829-38.

11 **Bruna, A., Rueda, O. M., Greenwood, W., Batra, A. S., Callari, M., Batra, R.**  
12 **N., Pogrebniak, K., Sandoval, J., Cassidy, J. W., Tufegdzc-Vidakovic, A. et al.**  
13 (2016). A Biobank of Breast Cancer Explants with Preserved Intra-tumor  
14 Heterogeneity to Screen Anticancer Compounds. *Cell* **167**, 260-274 e22.

15 **Byrne, A. T., Alferez, D. G., Amant, F., Annibaldi, D., Arribas, J., Biankin, A.**  
16 **V., Bruna, A., Budinska, E., Caldas, C., Chang, D. K. et al.** (2017). Interrogating  
17 open issues in cancer precision medicine with patient-derived xenografts. *Nat Rev*  
18 *Cancer* **17**, 254-268.

19 **Chen, P., Zuo, H., Xiong, H., Kolar, M. J., Chu, Q., Saghatelian, A.,**  
20 **Sieglwart, D. J. and Wan, Y.** (2017). Gpr132 sensing of lactate mediates tumor-  
21 macrophage interplay to promote breast cancer metastasis. *Proc Natl Acad Sci U S*  
22 *A* **114**, 580-585.

23 **Eckhardt, B. L., Parker, B. S., van Laar, R. K., Restall, C. M., Natoli, A. L.,**  
24 **Tavaria, M. D., Stanley, K. L., Sloan, E. K., Moseley, J. M. and Anderson, R. L.**  
25 (2005). Genomic analysis of a spontaneous model of breast cancer metastasis to  
26 bone reveals a role for the extracellular matrix. *Mol Cancer Res* **3**, 1-13.

27 **Fantozzi, A. and Christofori, G.** (2006). Mouse models of breast cancer  
28 metastasis. *Breast Cancer Res* **8**, 212.

1           **Francia, G., Cruz-Munoz, W., Man, S., Xu, P. and Kerbel, R. S.** (2011).  
2 Mouse models of advanced spontaneous metastasis for experimental therapeutics.  
3 *Nat Rev Cancer* **11**, 135-41.

4           **Frisch, S. M. and Screatton, R. A.** (2001). Anoikis mechanisms. *Curr Opin*  
5 *Cell Biol* **13**, 555-62.

6           **Guy, C. T., Cardiff, R. D. and Muller, W. J.** (1992a). Induction of mammary  
7 tumors by expression of polyomavirus middle T oncogene: a transgenic mouse  
8 model for metastatic disease. *Mol Cell Biol* **12**, 954-61.

9           **Guy, C. T., Webster, M. A., Schaller, M., Parsons, T. J., Cardiff, R. D. and**  
10 **Muller, W. J.** (1992b). Expression of the neu protooncogene in the mammary  
11 epithelium of transgenic mice induces metastatic disease. *Proc Natl Acad Sci U S A*  
12 **89**, 10578-82.

13           **Hanahan, D. and Weinberg, R. A.** (2011). Hallmarks of cancer: the next  
14 generation. *Cell* **144**, 646-74.

15           **Harney, A. S., Arwert, E. N., Entenberg, D., Wang, Y., Guo, P., Qian, B. Z.,**  
16 **Oktaý, M. H., Pollard, J. W., Jones, J. G. and Condeelis, J. S.** (2015). Real-Time  
17 Imaging Reveals Local, Transient Vascular Permeability, and Tumor Cell  
18 Intravasation Stimulated by TIE2hi Macrophage-Derived VEGFA. *Cancer Discov* **5**,  
19 932-43.

20           **Holen, I., Speirs, V., Morrissey, B. and Blyth, K.** (2017). In vivo models in  
21 breast cancer research: progress, challenges and future directions. *Dis Model Mech*  
22 **10**, 359-371.

23           **Hunter, K.** (2006). Host genetics influence tumour metastasis. *Nat Rev*  
24 *Cancer* **6**, 141-6.

25           **Janik, P., Briand, P. and Hartmann, N. R.** (1975). The effect of estrone-  
26 progesterone treatment on cell proliferation kinetics of hormone-dependent GR  
27 mouse mammary tumors. *Cancer Res* **35**, 3698-704.

1           **Johnstone, C. N., Smith, Y. E., Cao, Y., Burrows, A. D., Cross, R. S., Ling,**  
2 **X., Redvers, R. P., Doherty, J. P., Eckhardt, B. L., Natoli, A. L. et al. (2015).**  
3 Functional and molecular characterisation of EO771.LMB tumours, a new C57BL/6-  
4 mouse-derived model of spontaneously metastatic mammary cancer. *Dis Model*  
5 *Mech* **8**, 237-51.

6           **Khanna, C. and Hunter, K. (2005).** Modeling metastasis in vivo.  
7 *Carcinogenesis* **26**, 513-23.

8           **Lelekakis, M., Moseley, J. M., Martin, T. J., Hards, D., Williams, E., Ho, P.,**  
9 **Lowen, D., Javni, J., Miller, F. R., Slavin, J. et al. (1999).** A novel orthotopic model  
10 of breast cancer metastasis to bone. *Clin Exp Metastasis* **17**, 163-70.

11           **Lockman, P. R., Mittapalli, R. K., Taskar, K. S., Rudraraju, V., Gril, B.,**  
12 **Bohn, K. A., Adkins, C. E., Roberts, A., Thorsheim, H. R., Gaasch, J. A. et al.**  
13 (2010). Heterogeneous blood-tumor barrier permeability determines drug efficacy in  
14 experimental brain metastases of breast cancer. *Clin Cancer Res* **16**, 5664-78.

15           **Mahoney, K. H., Miller, B. E. and Heppner, G. H. (1985).** FACS quantitation  
16 of leucine aminopeptidase and acid phosphatase on tumor-associated macrophages  
17 from metastatic and nonmetastatic mouse mammary tumors. *J Leukoc Biol* **38**, 573-  
18 85.

19           **Miller, F. R., McEachern, D. and Miller, B. E. (1989).** Growth regulation of  
20 mouse mammary tumor cells in collagen gel cultures by diffusible factors produced  
21 by normal mammary gland epithelium and stromal fibroblasts. *Cancer Res* **49**, 6091-  
22 7.

23           **Morris, V. L., Tuck, A. B., Wilson, S. M., Percy, D. and Chambers, A. F.**  
24 (1993). Tumor progression and metastasis in murine D2 hyperplastic alveolar nodule  
25 mammary tumor cell lines. *Clin Exp Metastasis* **11**, 103-12.

26           **Neve, R. M., Chin, K., Fridlyand, J., Yeh, J., Baehner, F. L., Fevr, T., Clark,**  
27 **L., Bayani, N., Coppe, J. P., Tong, F. et al. (2006).** A collection of breast cancer cell  
28 lines for the study of functionally distinct cancer subtypes. *Cancer cell* **10**, 515-27.

1           **O'Reilly, M. S., Holmgren, L., Shing, Y., Chen, C., Rosenthal, R. A.,**  
2 **Moses, M., Lane, W. S., Cao, Y., Sage, E. H. and Folkman, J.** (1994). Angiostatin:  
3 a novel angiogenesis inhibitor that mediates the suppression of metastases by a  
4 Lewis lung carcinoma. *Cell* **79**, 315-28.

5           **Paoli, P., Giannoni, E. and Chiarugi, P.** (2013). Anoikis molecular pathways  
6 and its role in cancer progression. *Biochim Biophys Acta* **1833**, 3481-98.

7           **Shibue, T. and Weinberg, R. A.** (2009). Integrin beta1-focal adhesion kinase  
8 signaling directs the proliferation of metastatic cancer cells disseminated in the lungs.  
9 *Proc Natl Acad Sci U S A* **106**, 10290-5.

10           **Tester, A. M., Ruangpanit, N., Anderson, R. L. and Thompson, E. W.**  
11 (2000). MMP-9 secretion and MMP-2 activation distinguish invasive and metastatic  
12 sublines of a mouse mammary carcinoma system showing epithelial-mesenchymal  
13 transition traits. *Clin Exp Metastasis* **18**, 553-60.

14           **Viski, C., Konig, C., Kijewska, M., Mogler, C., Isacke, C. M. and Augustin,**  
15 **H. G.** (2016). Endosialin-Expressing Pericytes Promote Metastatic Dissemination.  
16 *Cancer Res* **76**, 5313-25.

17           **Xian, X., Hakansson, J., Stahlberg, A., Lindblom, P., Betsholtz, C.,**  
18 **Gerhardt, H. and Semb, H.** (2006). Pericytes limit tumor cell metastasis. *J Clin*  
19 *Invest* **116**, 642-51.

20           **Yang, J., Mani, S. A., Donaher, J. L., Ramaswamy, S., Itzykson, R. A.,**  
21 **Come, C., Savagner, P., Gitelman, I., Richardson, A. and Weinberg, R. A.** (2004).  
22 Twist, a master regulator of morphogenesis, plays an essential role in tumor  
23 metastasis. *Cell* **117**, 927-39.

24           **Yang, Y., Andersson, P., Hosaka, K., Zhang, Y., Cao, R., Iwamoto, H.,**  
25 **Yang, X., Nakamura, M., Wang, J., Zhuang, R. et al.** (2016). The PDGF-BB-SOX7  
26 axis-modulated IL-33 in pericytes and stromal cells promotes metastasis through  
27 tumour-associated macrophages. *Nat Commun* **7**, 11385.

1           Yang, Y., Yang, H. H., Hu, Y., Watson, P. H., Liu, H., Geiger, T. R., Anver,  
2 M. R., Haines, D. C., Martin, P., Green, J. E. et al. (2017). Immunocompetent  
3 mouse allograft models for development of therapies to target breast cancer  
4 metastasis. *Oncotarget* **8**, 30621-30643.

5           Zhang, X. H., Jin, X., Malladi, S., Zou, Y., Wen, Y. H., Brogi, E., Smid, M.,  
6 Foekens, J. A. and Massague, J. (2013). Selection of bone metastasis seeds by  
7 mesenchymal signals in the primary tumor stroma. *Cell* **154**, 1060-73.

8  
9  
10 **Figure Legends**

11  
12 **Fig. 1** Generation of syngeneic spontaneously metastatic D2A1 sublines. **A** Diagram  
13 outlining the strategy for selection of the metastatic sublines (see Methods and text  
14 for details). **B,C**  $5 \times 10^4$  D2A1, D2A1-m1 or D2A1-m2 cells were inoculated into the  
15 4th mammary fat pad of BALB/c mice (n = 5 - 6 mice per group). Growth of tumours  
16 in individual mice is shown. **B** Mice were culled between days 31 - 39 when the  
17 primary tumours reached a diameter of 12 - 14 mm (left panel). Metastatic burden in  
18 the lungs was monitored by % tumour area and number of lung nodules per lung  
19 section. Significant outliers are shown as white symbols. Data are mean values per  
20 mouse  $\pm$ s.e.m. Shown are representative images of lung metastases (arrowheads).  
21 Scale bar, 200  $\mu$ m. **C** Primary tumours were surgically excised when they reached ~6  
22 mm in diameter (day 13 - 15). All mice were culled on day 43 when the first mouse  
23 showed signs of ill health. Data shown are mean values per mouse  $\pm$ s.e.m. for  
24 primary tumour growth and metastatic burden in the lungs as assessed by % tumour  
25 area per lung section. Significant outliers are shown as white symbols.  
26 Representative images of lung sections are shown. Scale bar, 2mm.

27  
28 **Fig. 2** Spontaneous metastasis in an immunocompromised setting.  $5 \times 10^4$  D2A1 or  
29 D2A1-m2 cells were inoculated into the 4th mammary fat pad of NOD scid gamma  
30 (NSG) mice (n = 5 mice per group). **A** Mean tumour volume  $\pm$ s.e.m., non-significant  
31 at all time points. All mice were culled on day 28 when the first mouse showed signs  
32 of ill health. **B** Metastatic burden in the lung assessed as % tumour area and number  
33 of metastatic nodules per lung section. Shown are representative images. Data

1 shown are mean values per mouse  $\pm$ s.e.m. Significant outlier is shown as white  
2 symbol. Scale bar, 2 mm.

3

4 **Fig. 3** Experimental metastasis assays. **A**  $4 \times 10^5$  D2A1, D2A1-m1 or D2A1-m2 cells  
5 were inoculated via the tail vein into BALB/c mice (n = 8 mice per group). 11 days  
6 later, lungs were removed at necropsy. Data show quantification of tumour burden as  
7 monitored by % tumour area and number of lung nodules per lung section. Right  
8 panel, representative lung images. Scale bar, 2 mm. **B**  $2 \times 10^5$  D2A1-Luc, D2A1-m1-  
9 Luc or D2A1-m2-Luc cells were inoculated into the left ventricle of BALB/c mice (n =  
10 6 mice per group). 10 days later, bones and brains were removed at necropsy and  
11 IVIS imaged *ex vivo*. Representative *ex vivo* bone IVIS images are shown. Scale bar,  
12 1 cm. **C**  $2 \times 10^5$  D2A1-Luc, D2A1-m1-Luc or D2A1-m2-Luc cells were inoculated into  
13 the spleen of BALB/c mice (n = 8 mice per group). 13 days later livers were removed  
14 at necropsy and IVIS imaged *ex vivo*. Shown are representative IVIS images Scale  
15 bar, 1 cm. Significant outliers are shown as white symbols. All data are mean values  
16 per mouse  $\pm$ s.e.m.

17

18 **Fig. 4** Characterisation of the D2A1 metastatic sublines *in vitro*. **A** Upper panel,  
19 phase contrast images of D2A1, D2A1-m1 and D2A1-m2 cells. Scale bar, 200  $\mu$ m.  
20 Lower panel, cells cultured on coverslips were stained with Alexa488-phalloidin and  
21 DAPI. Scale bar, 100  $\mu$ m. Data shows mean values (n = 6 samples per cell line)  
22  $\pm$ s.e.m. of cell roundness (see Methods). Equivalent results were obtained on 2  
23 separate occasions. **B** Colony formation assay. Data shows mean number of  
24 colonies and average colony area  $\pm$ s.e.m., n = 3 wells per cell line. Representative  
25 images of crystal violet stained wells are shown below. Equivalent results were  
26 obtained on 3 separate occasions. **C** Cell proliferation monitored using the IncuCyte  
27 Live-Cell Analysis System. Data shown are mean values  $\pm$ s.d., n = 6 wells per cell  
28 line. Equivalent results were obtained on 2 separate occasions. **D** Cell viability  
29 measured by CellTiter-Glo at the indicated time points. Data shown are mean values  
30  $\pm$ s.d., n = 6 wells per cell line per time point. Equivalent results were obtained on 2  
31 separate occasions. **E** Wound healing assay monitored using the IncuCyte Live-Cell  
32 Analysis System. Data represents % wound closure  $\pm$ s.d., n = 8 wells per cell line.  
33 Shown are representative false coloured images of cells time at 0 and at 24 hours.  
34 Scale bar, 300  $\mu$ m. **F** Transwell chemotaxis assay. Data shown are mean values  
35  $\pm$ s.e.m. (n = 3) for cells transmigrated to the lower side of the filter relative to the  
36 initial plated cells. **C-F** Statistical differences were determined using 2-way ANOVA  
37 and Bonferroni post-hoc testing, with time and cell lines as independent variables. In



1 all cases both D2A1-m1 and D2A1-m2 are significantly different to the parental D2A1  
2 cells ( $P < 0.0001$ ).

3

4 **Fig. 5** Characterisation of the D2A1 metastatic sublines in non-adherent culture. **A**  
5 D2A1, D2A1-m1 and D2A1-m2 cells were plated onto adherent tissue culture or non-  
6 adherent 6-well plates and apoptosis monitored 24 hours later by annexin V/PI  
7 staining. Data shows the proportions of live (AV-/PI-), early apoptotic (AV+/PI-), late  
8 apoptotic (AV+/PI+) and necrotic (AV-/PI+) cells, mean of 3 experiments  $\pm$ s.e.m.,  $n =$   
9 3 per cell line per experiment. D2A1 cells had significantly less viable cells compared  
10 to D2A1-m1 ( $P = 0.0114$ ) and D2A1-m2 ( $P = 0.0119$ ) cells. **B** Spheroid assay. Cells  
11 were plated in U bottom low adherence plates ( $n = 6$  per cell line) and cultured for 14  
12 days. At stated time points, cell viability in the tumour spheroids was monitored by  
13 CellTiter-Glo, mean values  $\pm$ s.e.m. Examples of tumour spheroid at day 14 are  
14 shown. Scale bar, 400  $\mu$ m. Equivalent results were obtained on 2 separate occasions.  
15 **c** Invasion into a 3D collagen matrix. Spheroids were embedded into collagen and  
16 single cell invasion was monitored 24, 48 and 72 hours later by measuring the mean  
17 square displacement (MSD). Data shown are mean values  $\pm$ s.e.m.,  $n = 3 - 6$   
18 spheroids per time point. Representative images at 48 hours are shown. Scale bar,  
19 400  $\mu$ m. All panels, statistical differences were determined using 2-way ANOVA and  
20 Bonferroni post-hoc testing. Equivalent results were obtained on 2 separate  
21 occasions.

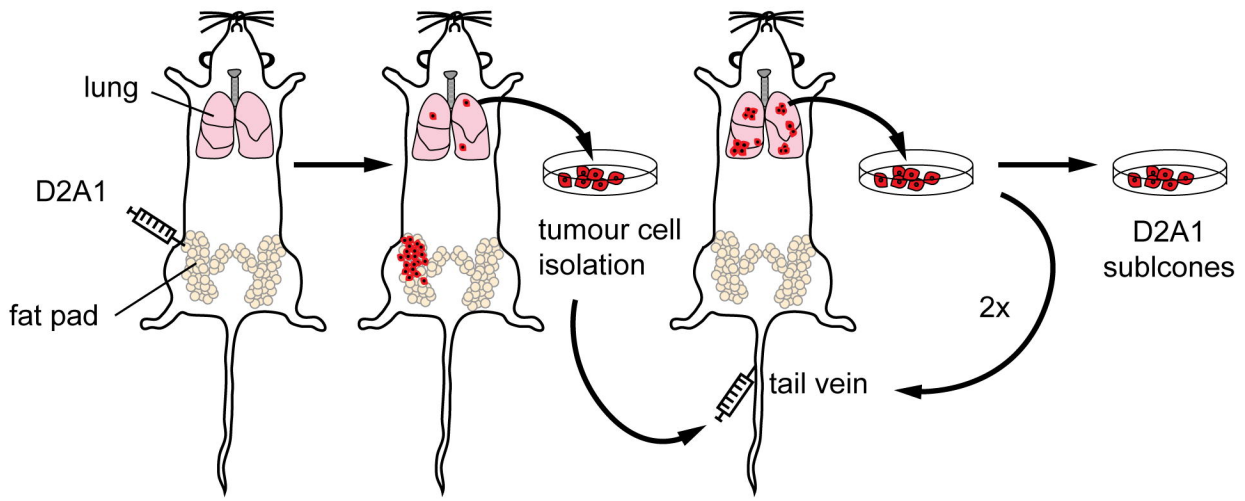
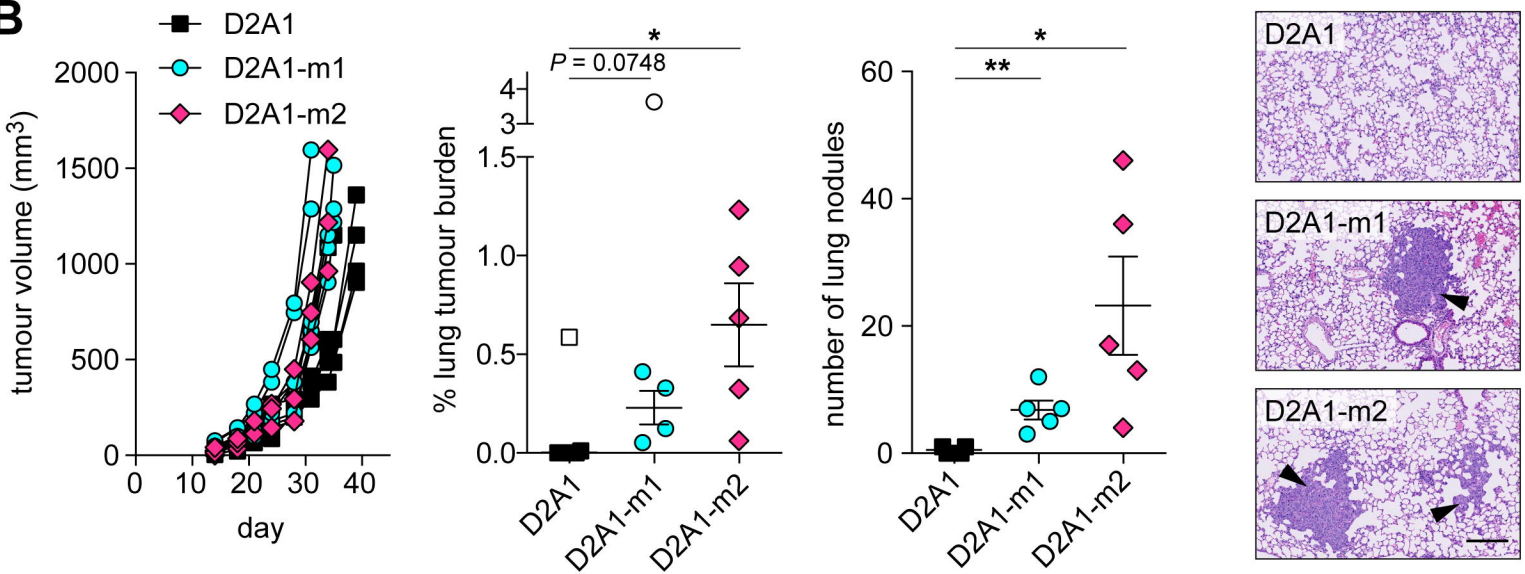
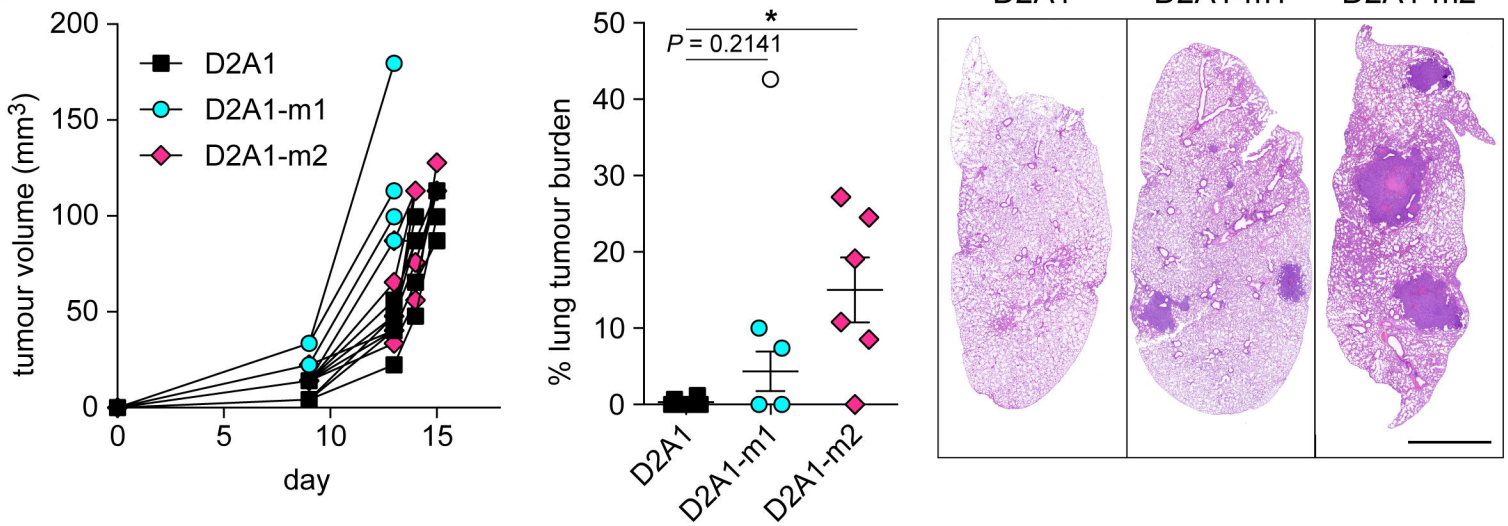
22

23 **Fig. 6** Stromal cell recruitment in primary tumours. **A, B** Primary tumours from the  
24 spontaneous metastasis experiments shown in Fig. 1B and Fig. 2 were sectioned  
25 and stained for the  $\alpha$ SMA or endomucin. **A** BALB/c mice from Fig. 1B, **B** NSG mice  
26 from Fig. 2. Left panels, representative images. Scale bar, 100  $\mu$ m. Right panels,  
27 quantification of staining from at least 4 tumours per group  $\pm$ s.e.m. ( $n > 6$  fields of  
28 view per tumour). Significant outlier is shown as white symbol. **C** Competitive  
29 fibroblast attraction assay (see Supplementary Figure S4A for experimental set up).  
30 Migration of individual 3T3 cells towards D2A1 vs. D2A1, D2A1 vs. D2A1-m1 or  
31 D2A1 vs. D2A1-m2 cells was monitored over 8 hours ( $n > 60$  cells tracked/sample).  
32 Left panel, percentage net displacement of fibroblasts (see Supplementary Figure  
33 S4B for individual cell tracks and quantification). Middle and right panels, velocity  
34 ( $\mu$ m/min) and Euclidean distance ( $\mu$ m) of fibroblast migration. Box and whisker  
35 graphs, box extends from the 25th to 75th percentiles, middle line plotted at median,  
36 whiskers are minimum and maximum, + indicates mean of data. **D** Fibroblast  
37 contraction assay. Data shown are % contraction of the fibroblast containing

1 Matrigel/collagen gel after 14 days treatment with DMEM, TGF $\beta$  or conditioned  
2 medium from D2A1, D2A1-m1 and D2A1-m2 cells, n = 2 wells/condition.  
3 Representative images of the gels are shown.

4

5 **Fig. 7** Gene expression profiling. RNA was isolated from independent biological  
6 replicates (D2A1.1, .2 and .3; D2A1-m1.1 and .2; D2A1-m2.1, .2 and .3) and subject  
7 to gene expression profiling. **A** Principle component analysis estimating the relations  
8 of D2A1, D2A1-m1 and D2A1-m2 cells based on the genes with coefficient of  
9 variance > 0.1 across the 8 samples. **B** Upper panel, number of differentially  
10 expressed genes ( $p < 0.001$ ,  $\geq 1.5$ -fold change). Lower panel, number of unique and  
11 shared differentially expressed genes between D2A1-m1 and D2A1-m2 sublines.  
12 Venn diagram depicting percentages. **C** Dendrogram shows correlation-centred  
13 hierarchical clustering based on average linkage. Shown are tumour cell expression  
14 data of 481 genes that were significantly differentially expressed between D2A1 and  
15 D2A1-m1 or D2A1 and D2A1-m2 cells with  $\geq 1.5$ -fold change,  $p < 0.001$ . **D** Top  
16 canonical pathways changed between D2A1-m1 and D2A1 as well as D2A1-m2 and  
17 D2A1 identified using IPA ( $p < 0.05$ ) based on the differentially expressed genes ( $p <$   
18  $0.001$ ,  $\geq 1.5$ -fold change).

**Figure 1****A****B****C**

**Figure 2**

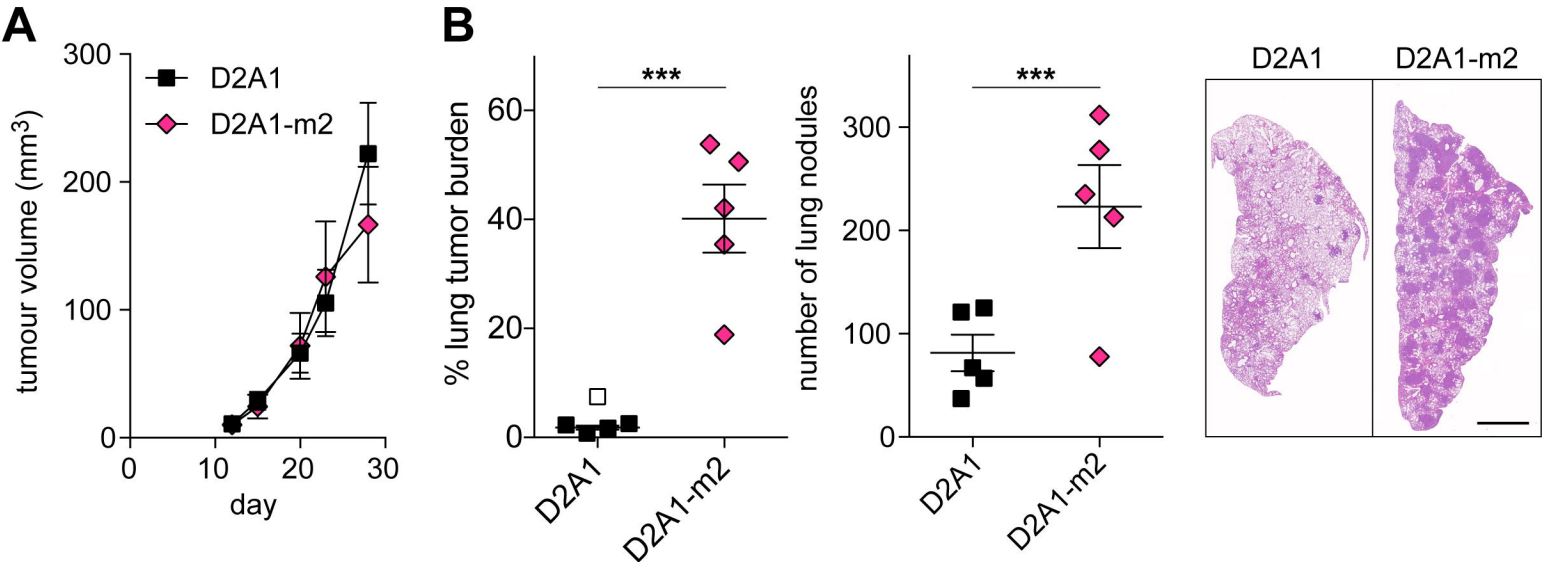
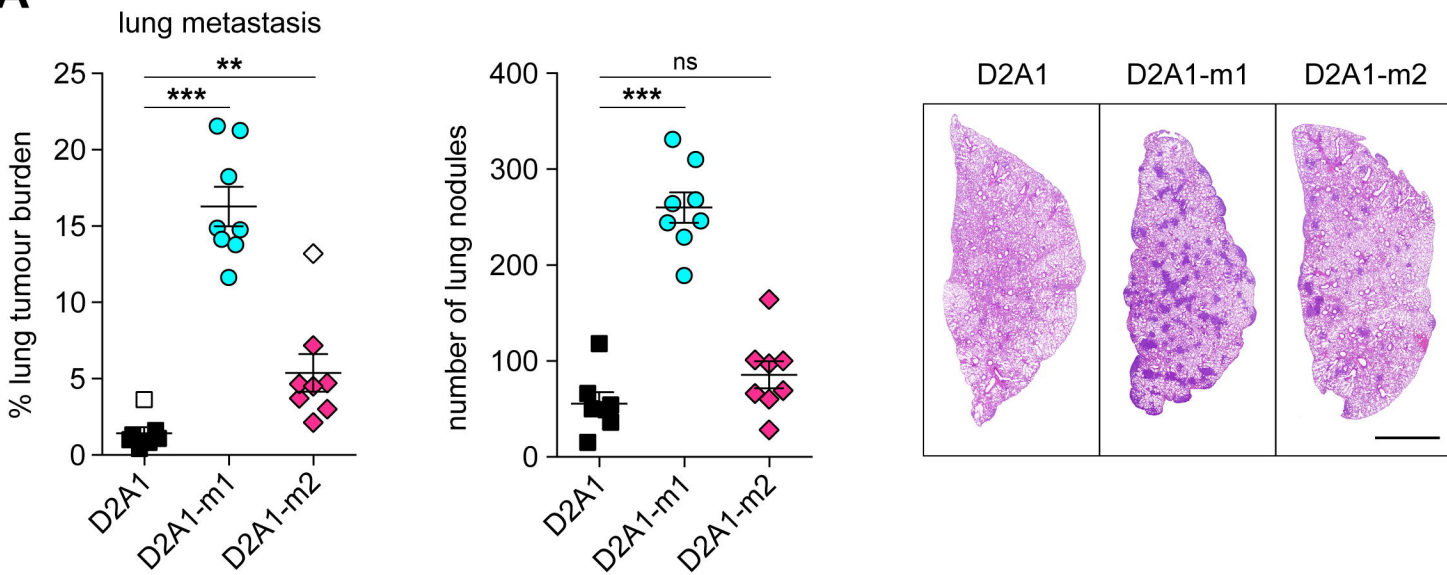
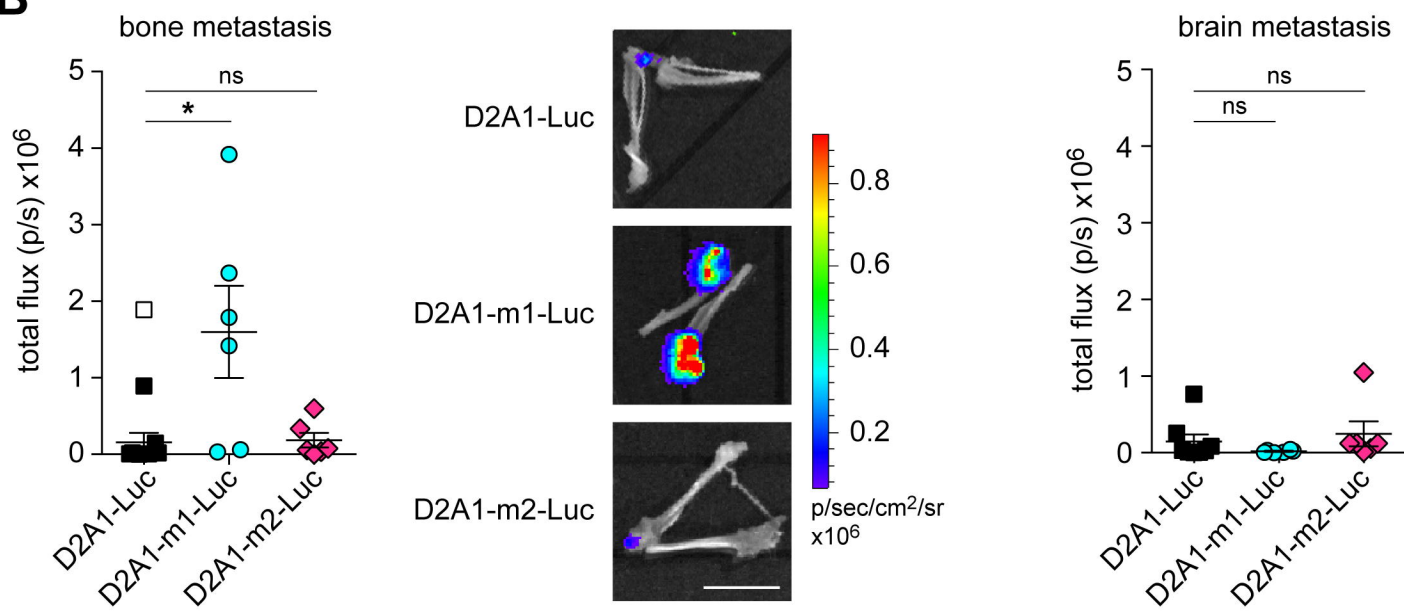


# Figure 3

**A**



**B**



**C**

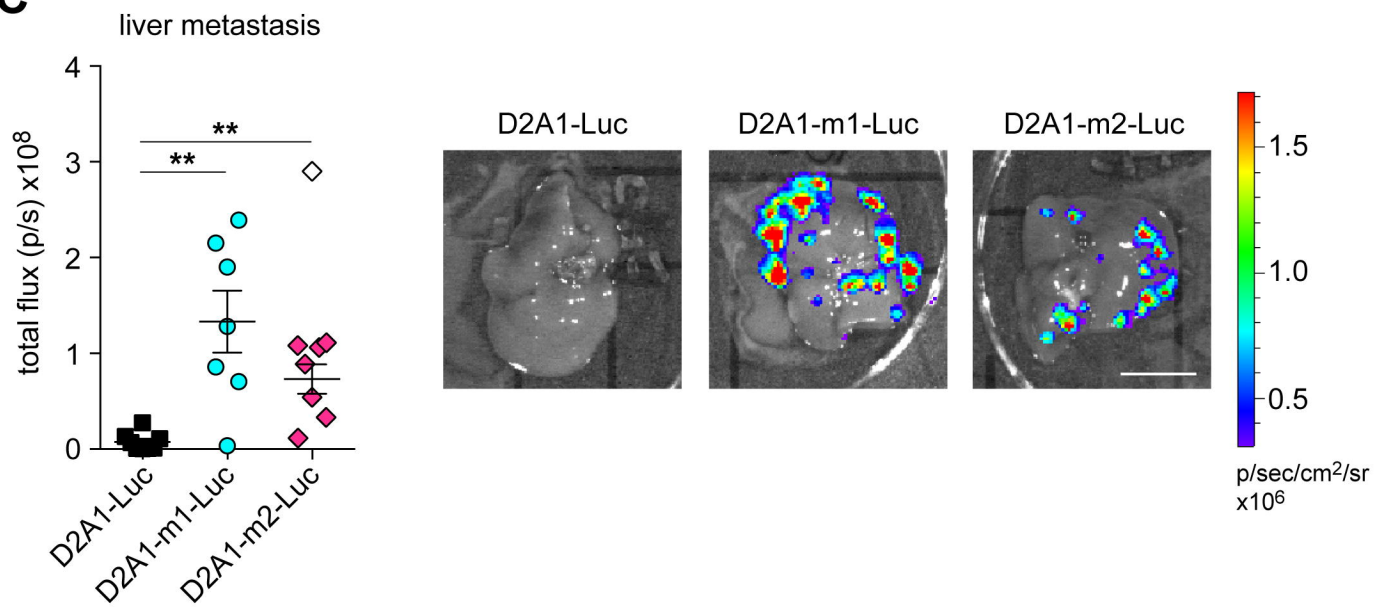
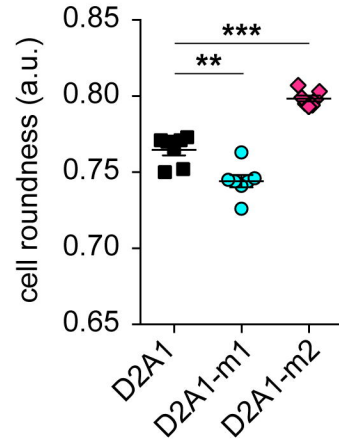
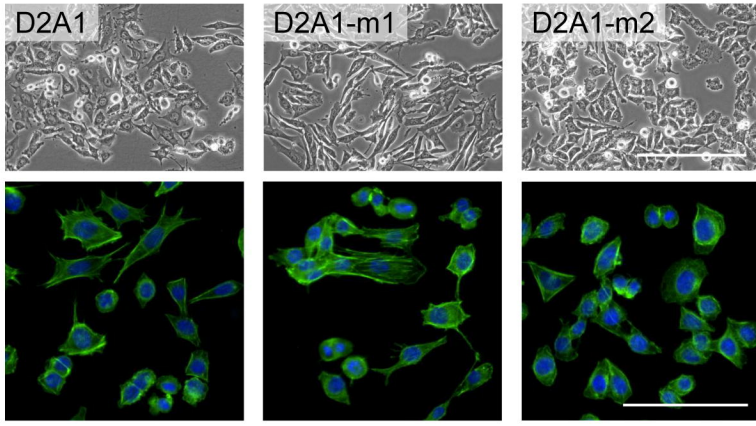
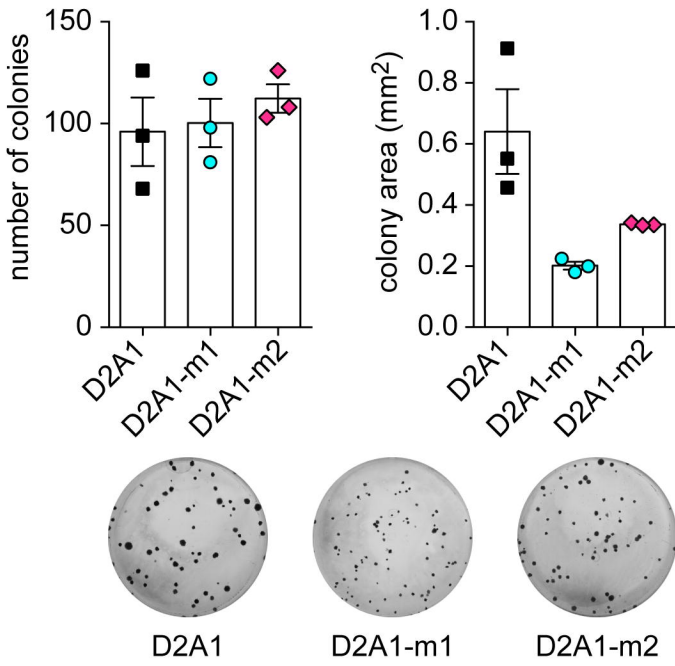


# Figure 4

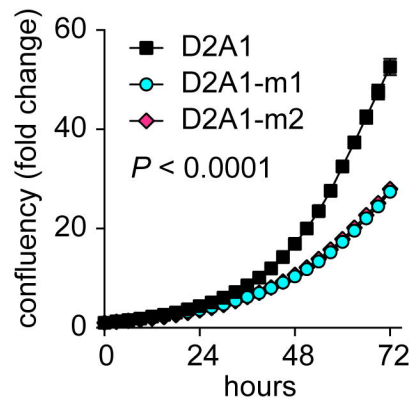
**A**



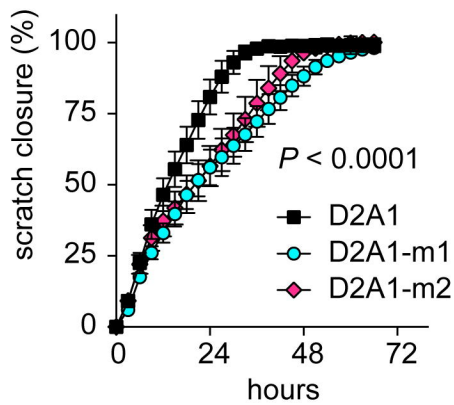
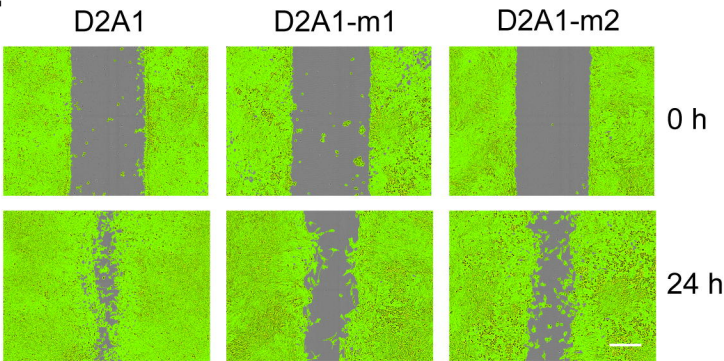
**B**



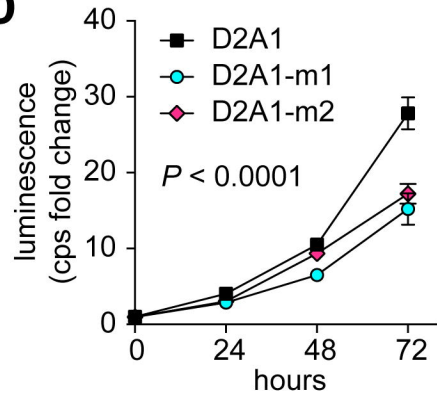
**C**



**E**



**D**



**F**

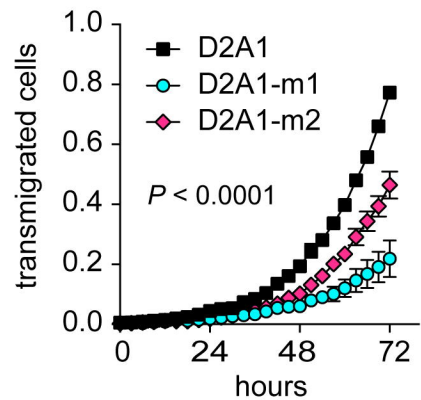
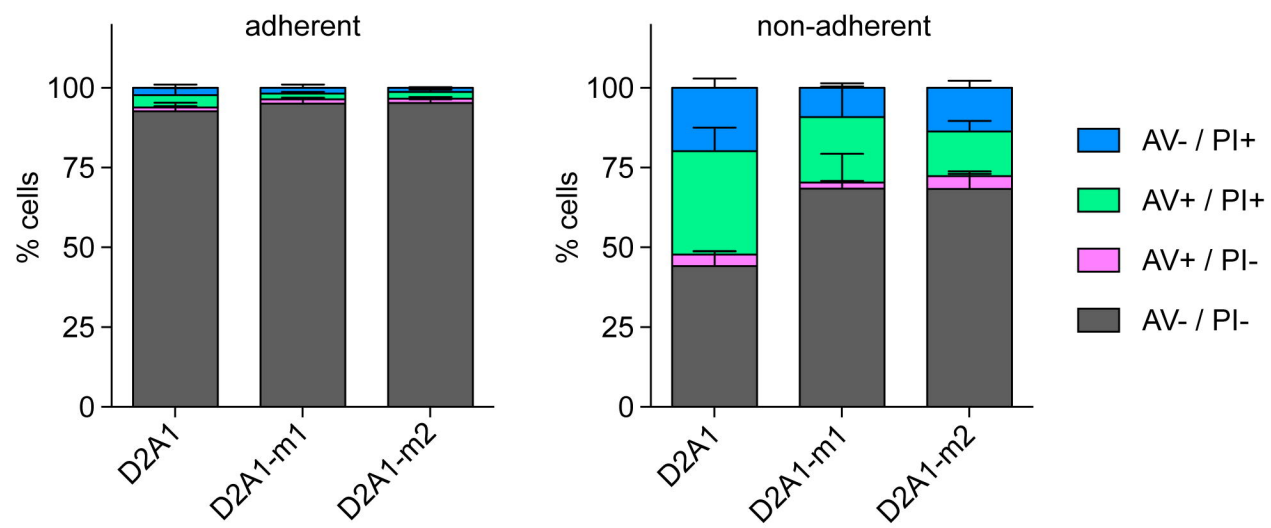
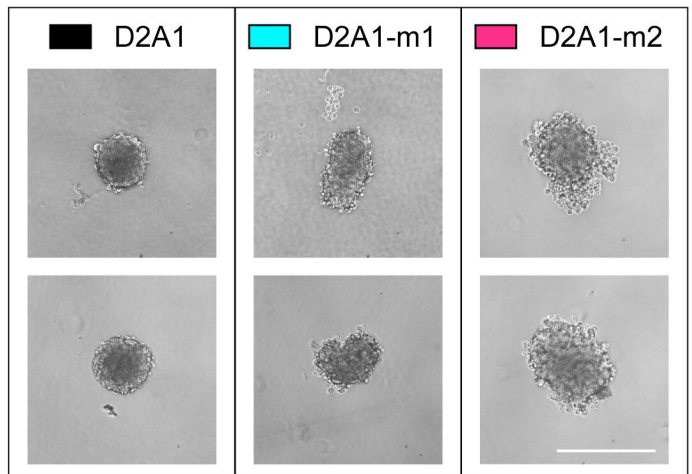
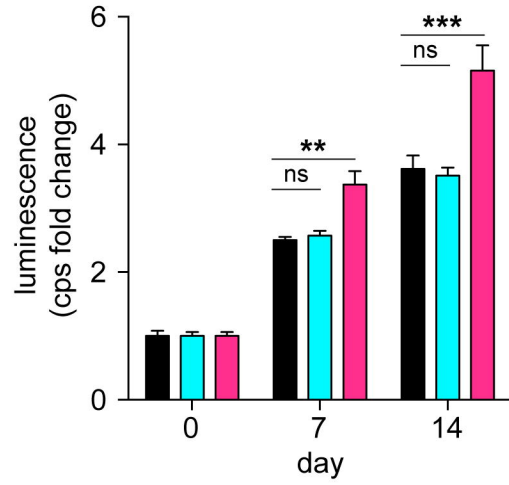


**Figure 5**

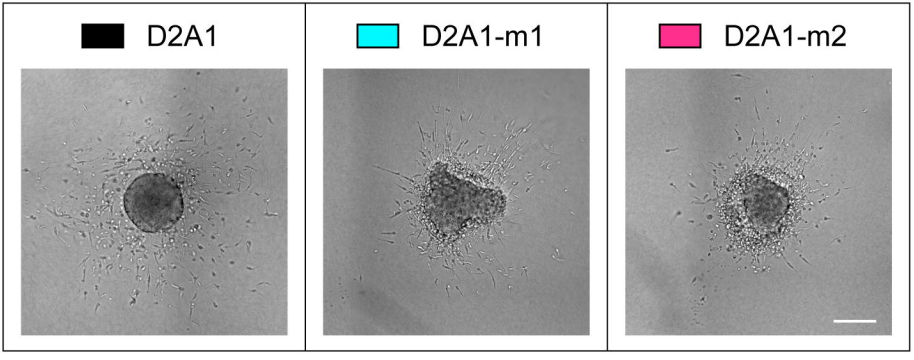
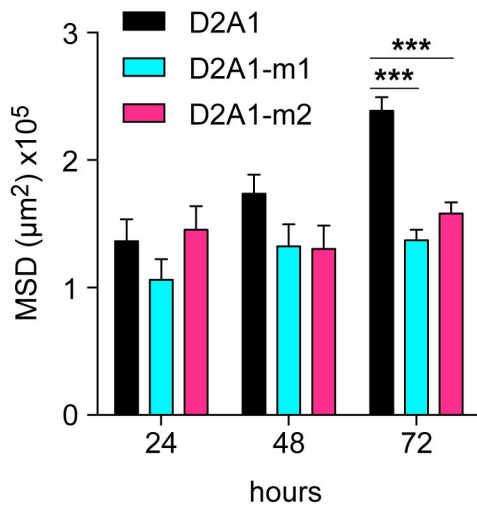
**A**

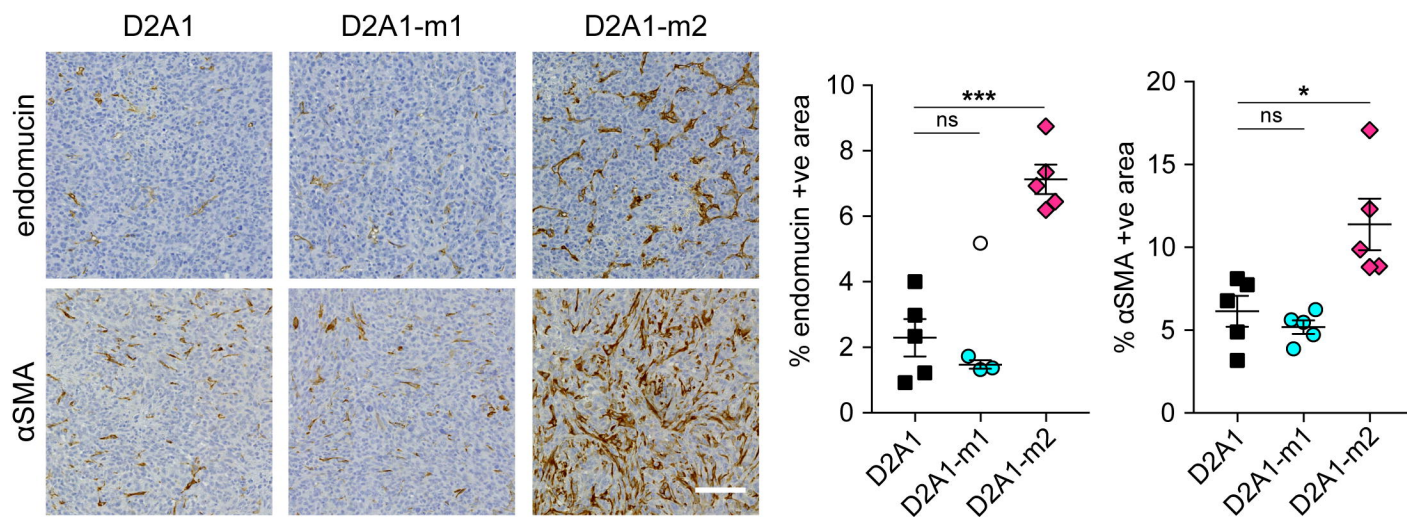
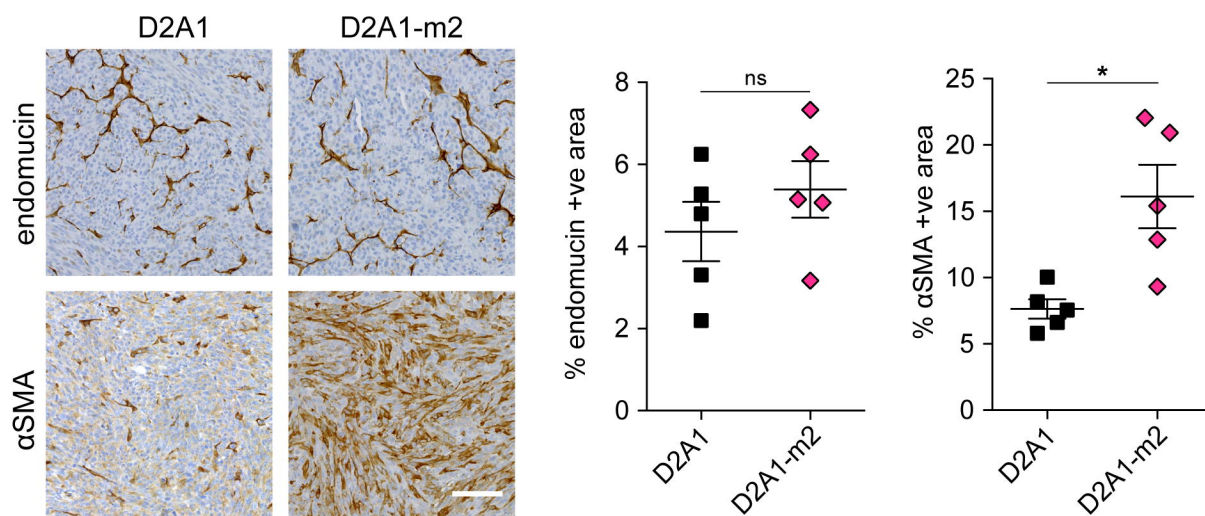
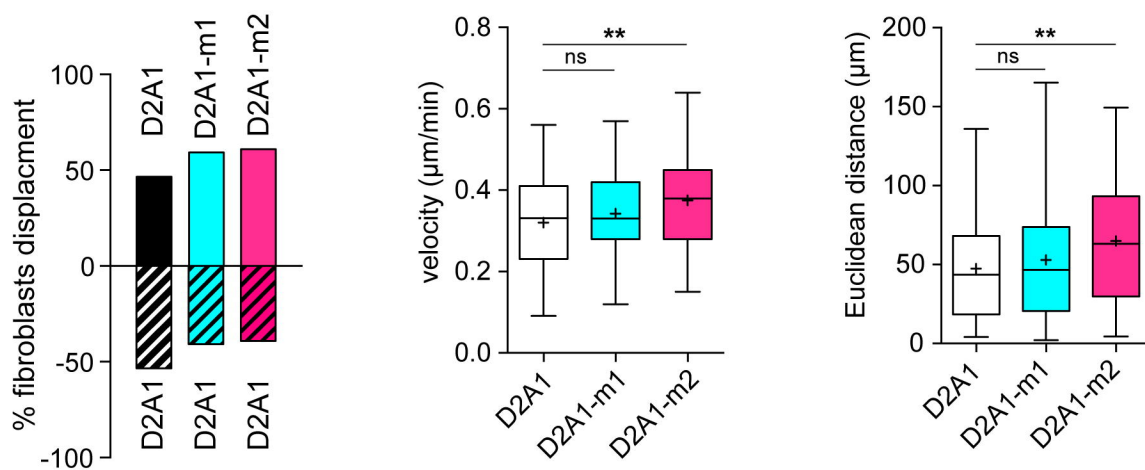
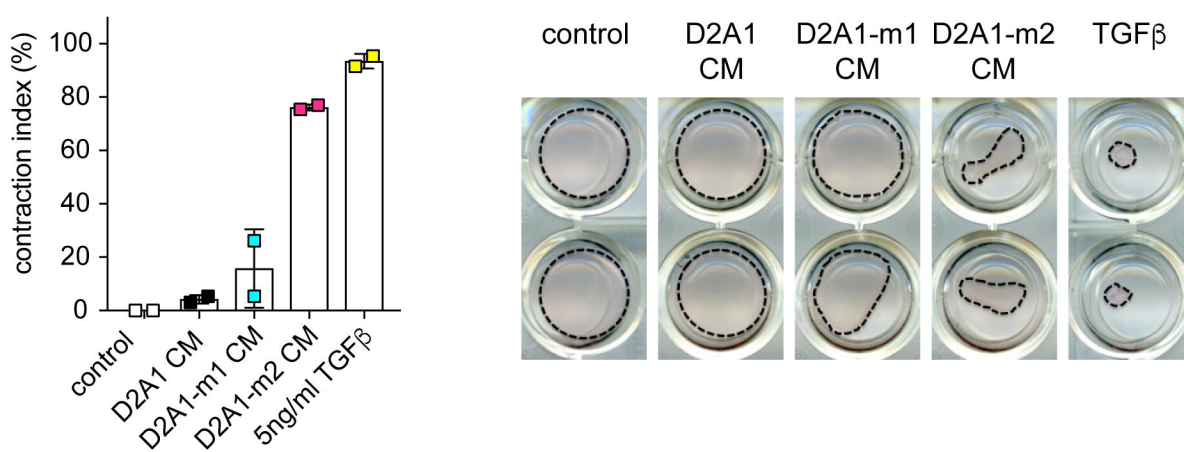


**B**

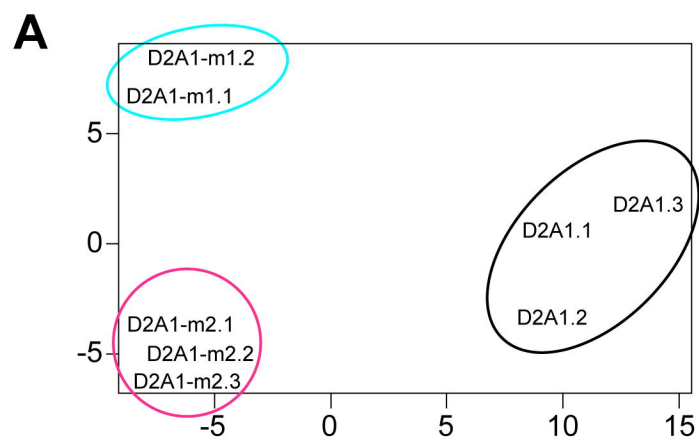


**C**



**Figure 6****A****B****C****D**



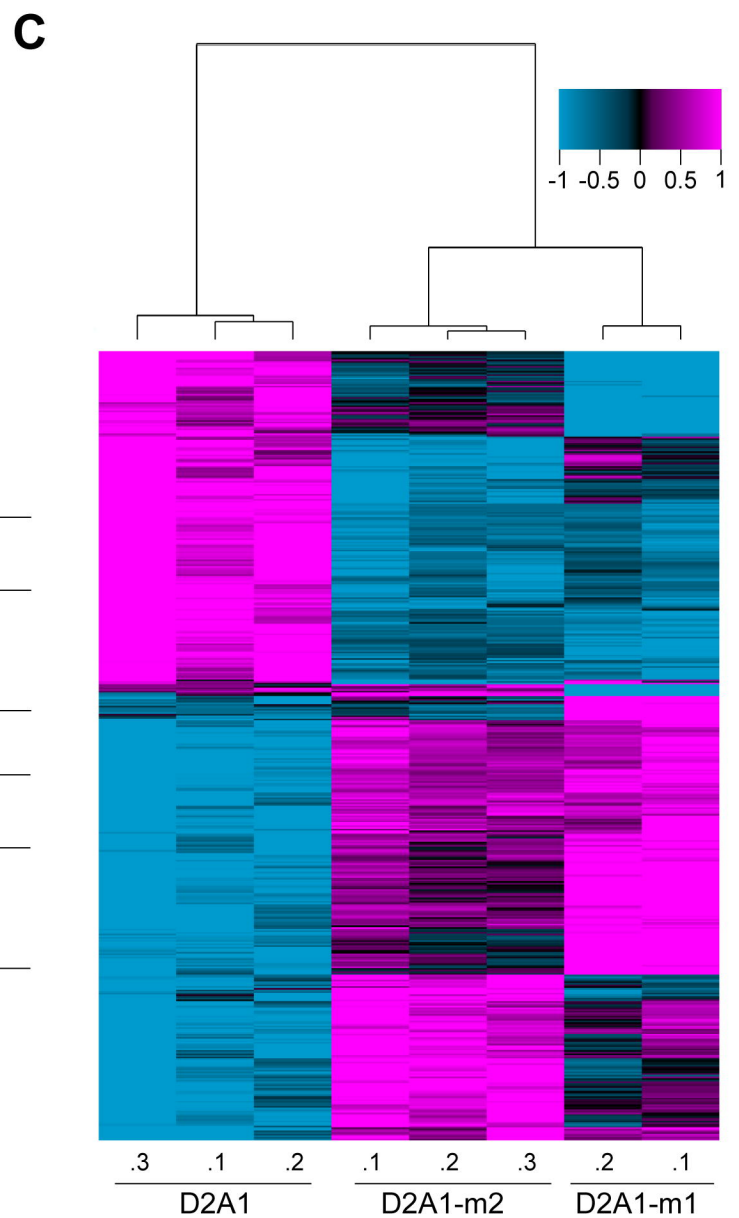
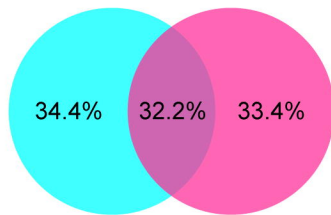
**Figure 7**

**B**

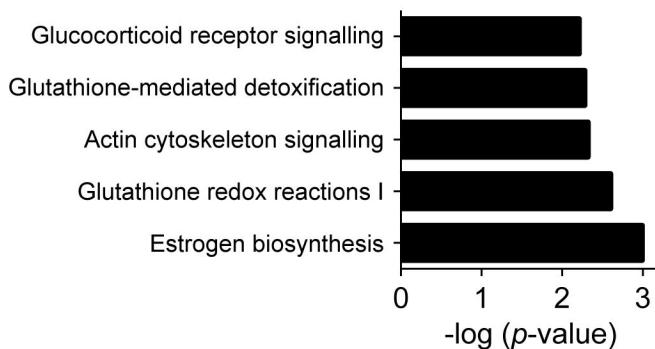
	D2A1-m1 vs D2A1	D2A1-m2 vs D2A1
sign. changes > 1.5 fold	323	318
up-regulated genes	176	178
down-regulated genes	147	140

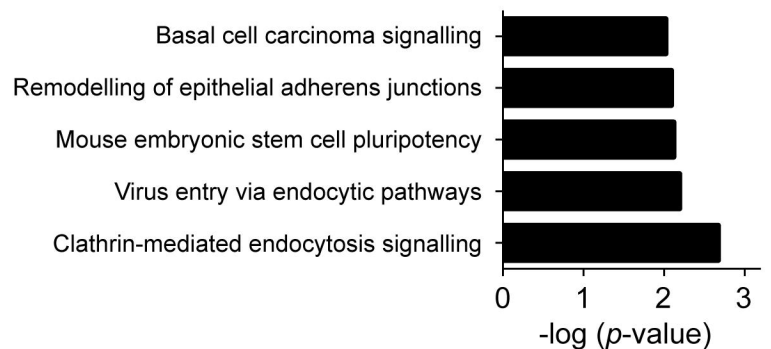
	number of genes
genes changed in both m1 & m2	156
genes only changed in m1	167
genes only changed in m2	162



**D** Top canonical pathways D2A1-m1 vs. D2A1



Top canonical pathways D2A1-m2 vs. D2A1



**Generation and characterisation of two D2A1 mammary cancer sublines to model spontaneous and experimental metastasis in a syngeneic BALB/c host**

Ute Jungwirth, Antoinette van Weverwijk, Miriam J. Melake, Ann F. Chambers,  
Qiong Gao, Marc Fivaz and Clare M. Isacke

**Supplementary Material**

**Supplementary Figure S1**

**Supplementary Figure S2**

**Supplementary Figure S3**

**Supplementary Figure S4**

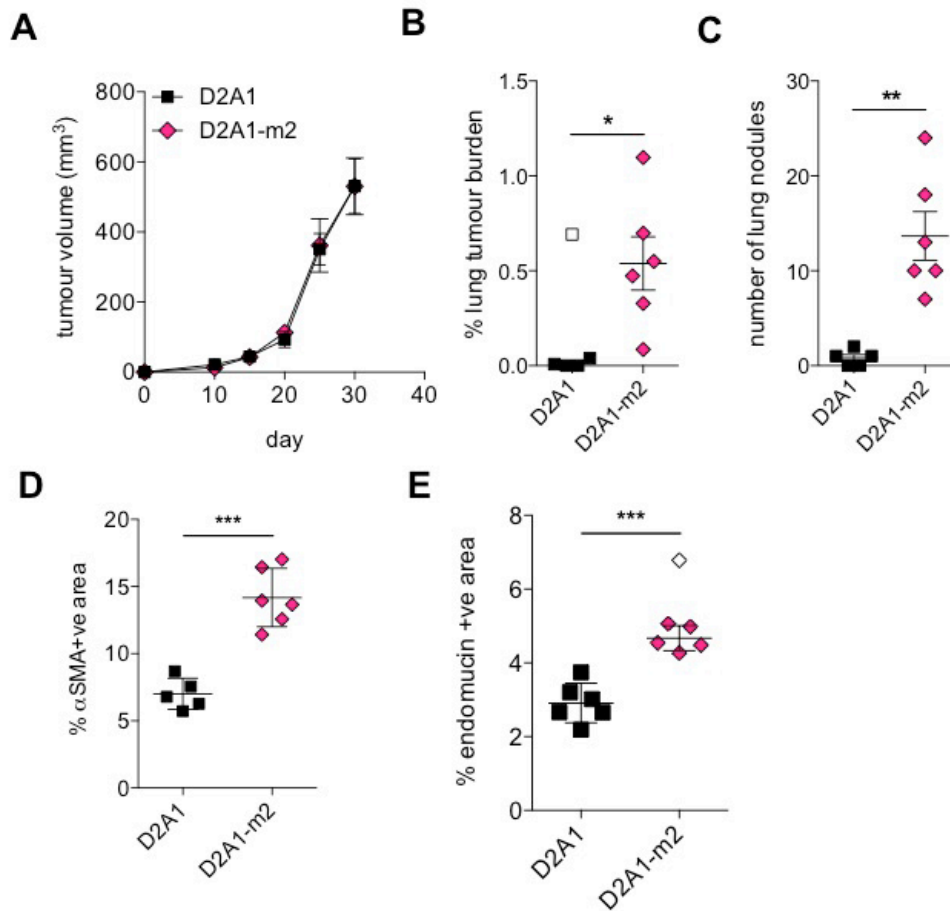
**Supplementary Table S1**

**Supplementary Table S2**

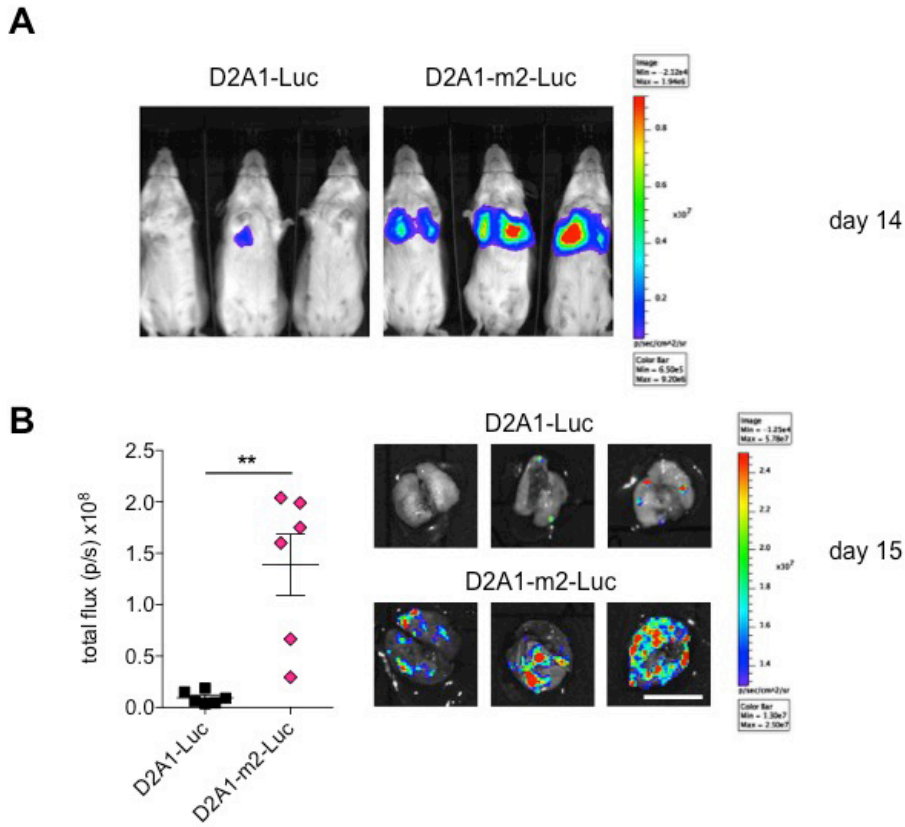
**Supplementary Table S3**

**Supplementary Table S4**

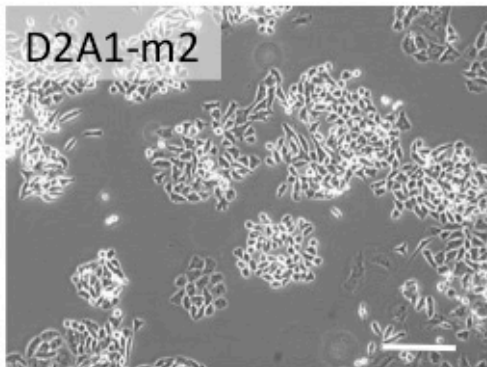
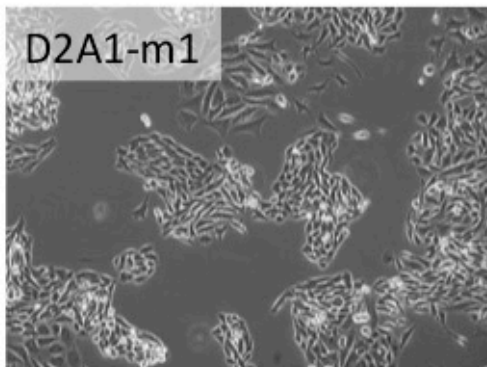
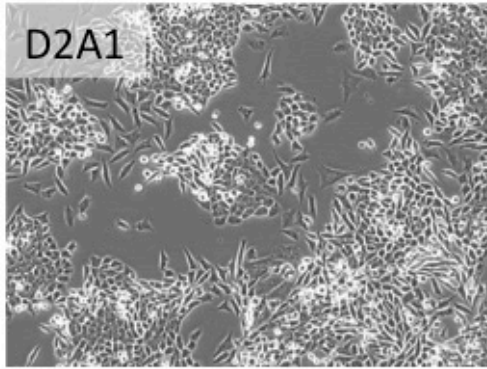
**Supplementary Table S5**



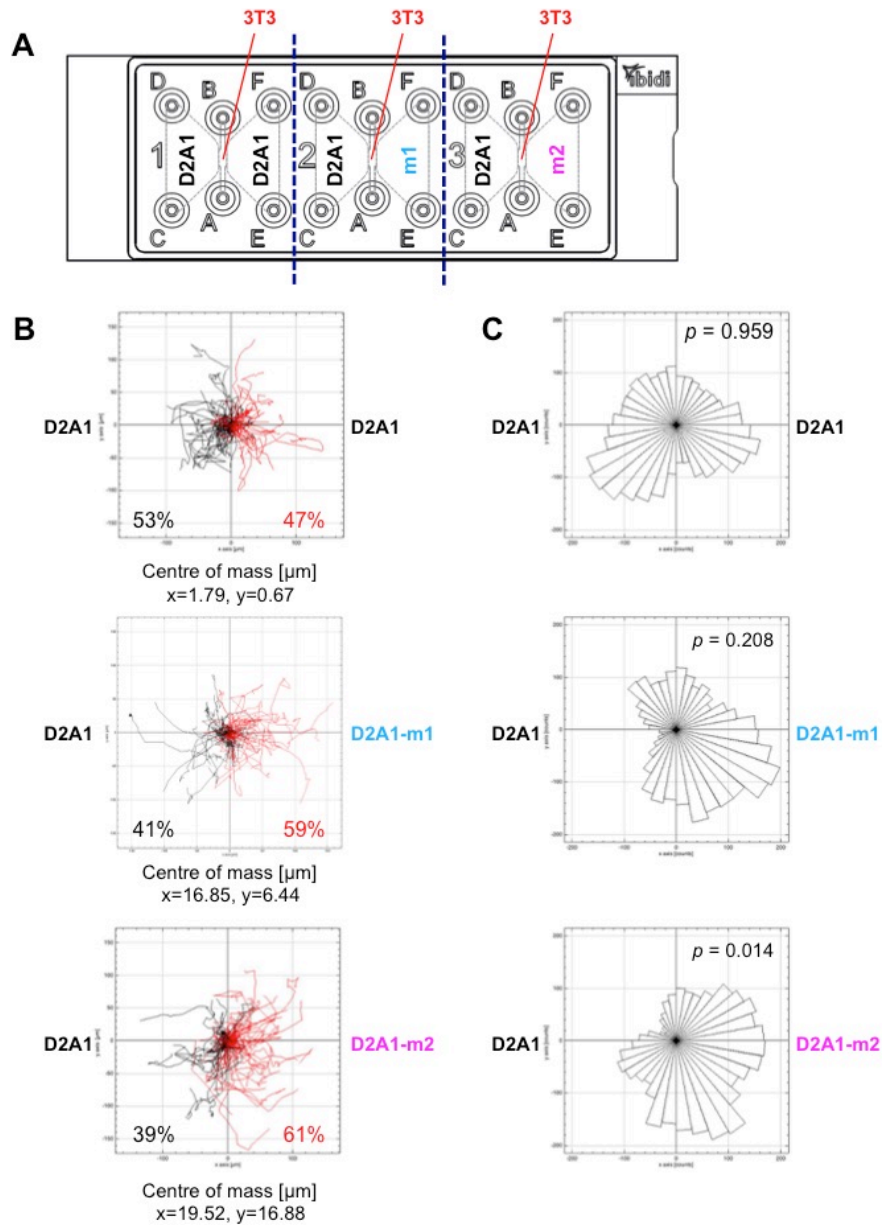
**Supplementary Figure S1** Spontaneous metastasis assay in BALB/c mice.  $5 \times 10^4$  D2A1 or D2A1-m2 cells were inoculated into the 4th mammary fat pad of BALB/c mice ( $n = 5$  or  $6$  mice per group) and culled on day 30. **A** Primary tumour growth. **B,C** Spontaneous metastasis to the lung assessed by % tumour burden and number of metastatic nodules per lung section. Data shown are mean values per mouse  $\pm$  SEM. **D,E** Primary tumours were sectioned and stained for **D** the activated fibroblast marker  $\alpha$ SMA, or **E** the endothelial marker endomucin. Data shows quantification of staining of 6 tumours per group  $\pm$  s.e.m. ( $n > 6$  fields of view per tumour).



**Supplementary Figure S2** Experimental lung metastasis assay with luciferase tagged cells.  $4 \times 10^5$  D2A1-Luc or D2A1-m2-Luc cells were inoculated intravenously into BALB/c mice ( $n = 6$  mice per group). **A** Representative *in vivo* IVIS imaging on day 14. **B** Mice were culled on day 15 when the first mouse showed signs of ill health. Quantification of tumour burden in the lungs via *ex vivo* IVIS imaging. Mean values per mouse  $\pm$ s.e.m.. Representative *ex vivo* lung IVIS images are shown. Scale bar, 1 cm.



**Supplementary Figure S3** Phase contrast images of D2A1, D2A1-m1 and D2A1-m2 cells grown on tissue culture plastic. Scale bar, 400  $\mu\text{m}$ .



**Supplementary Figure S4** Competitive fibroblasts migration assay. **A** Diagram of the experimental setup for the 'ibidi'  $\mu$ -slide chemotaxis system. Following the manufacturer's instructions, fibroblasts were injected into the central viewing chamber via port A. 3 hours later, D2A1 cells were injected into the left reservoir via port C and either D2A1, D2A1-m1 or D2A1-m2 cells were injected into the right reservoir via port E. Fibroblast migration in the central chamber was imaged over 8 hours (see Methods for further details). **B** Paths taken by individual 3T3 fibroblasts, where all initial starting positions ( $t=0$ ) are plotted at the origin ( $x=0$ ,  $y=0$ ). Red indicates paths with a positive net displacement towards tumour cells seeded on the right hand side. Black paths indicate net displacement towards the left. The percentage of cells exhibiting movement to the left (black) or right (red) is indicated and shown graphically in Fig. 6C, left panel. Coordinates of centre of mass are given below the panels. **C** Corresponding circular histograms, with  $p$ -values calculated using the Rayleigh test for vector data. Only D2A1-m2 cells induce a significant inhomogeneous distribution of fibroblast trajectories.

**Supplementary Table S1.** Top 40 genes differentially expressed in D2A1-m1 cells vs. D2A1 cells

Symbol	Gene name	Accession Number	Fold change	Parametric p-value
Mgp	Matrix Gla protein	NM_008597	16.95	< 1e-07
Arhgdib	Rho, GDP dissociation inhibitor beta	NM_007486	13.33	5.10E-05
Fgf7	Fibroblast Growth Factor 7	NM_008008	12.35	1.71E-05
Itgbl1	Integrin Subunit Beta Like 1	NM_145467	6.67	2.21E-05
Thbs2	Thrombospondin 2	NM_011581	6.25	1.30E-06
Pdgfrl	Platelet-derived growth factor receptor-like	NM_026840	5.88	2.70E-06
Id4	Inhibitor of DNA binding 4	NM_031166	5.88	7.40E-06
Tnfrsf11b	TNF receptor superfamily member 11b	NM_008764	5.56	2.93E-05
Lgals7	Galectin 7	NM_008496	5.56	3.59E-05
Akr1c18	Aldo-keto reductase family 1, member C18	NM_134066	5.00	2.40E-06
Ly6a	Lymphocyte antigen 6 complex, locus A	NM_010738	5.00	4.80E-06
Tpm2	Tropomyosin 2, beta	NM_009416	5.00	1.10E-05
Chst1	Carbohydrate (keratan sulfate Gal-6) sulfotransferase 1	NM_023850	4.17	5.00E-07
Ifi27	Interferon, alpha-inducible protein 27	NM_029803	4.17	8.64E-04
AA467197		NM_001004174	4.00	3.00E-07
Casp1	Caspase 1	NM_009807	4.00	6.88E-04
Aqp1	Aquaporin 1	NM_007472	3.45	5.17E-05
Krt8	Keratin 8	NM_031170	3.45	1.19E-04
Ptrf	Caveolae associated 1	NM_008986	3.23	2.70E-05
Vcam1	Vascular cell adhesion molecule 1	NM_011693	3.23	4.65E-04
Aqp5	Aquaporin 5	NM_009701	3.13	4.00E-07
Ank	Progressive ankylosis	NM_020332	3.03	1.00E-07
Idb4	Inhibitor of DNA binding 4	AK041164	3.03	7.50E-06
Aldh3a1	Aldehyde dehydrogenase 3 family member A1	NM_007436	3.03	4.91E-05
Lxn	Latexin	NM_016753	2.94	3.20E-06
D14Ertd668e	PHD finger protein 11D	NM_199015	2.70	5.70E-06
Tmem86a	Transmembrane protein 86A	NM_026436	2.70	1.77E-05
LOC100046616		XM_001476512	2.63	2.00E-07
A1467606		NM_178901	2.63	1.28E-05
Ecm1	Extracellular matrix protein 1	NM_007899	2.63	1.61E-04
Cgn	Cingulin	XM_001001375	-2.59	1.10E-06
Tuft1	Tuftelin 1	NM_011656	-2.59	4.90E-05
Ak3	Adenylate kinase 3	NM_021299	-2.87	1.61E-04
Bgn	Biglycan	NM_007542	-2.98	3.05E-05
1810015A11 Rik	YdjC homolog	NM_026940	-3.01	5.45E-05
Ogn	Osteoglycin	NM_008760	-3.10	5.62E-05
Tpd52	Tumor protein D52	NM_009412	-3.15	5.40E-06
Chchd10	Coiled-coil-helix-coiled-coil-helix domain containing 10	NM_175329	-3.52	4.25E-04
4732462B05 Rik		AK028848	-4.13	1.85E-05
Ptx3	Pentraxin related gene	NM_008987	-4.85	3.93E-05

**Supplementary Table S2.** Top 40 genes differentially expressed in D2A1-m2 cells vs. D2A1 cells

Symbol	Gene name	Accession number	Fold change	Parametric p-value
Casp1	Caspase 1	NM_009807	10.99	4.30E-06
Arhgdib	Rho, GDP dissociation inhibitor beta	NM_007486	10.99	1.22E-05
Lgals7	Galectin 7	NM_008496	9.09	7.00E-07
Fgf7	Fibroblast Growth Factor 7	NM_008008	7.69	6.40E-06
Itgb1	Integrin Subunit Beta Like 1	NM_145467	5.00	6.20E-06
Tpm2	Tropomyosin 2, beta	NM_009416	4.76	6.50E-06
Mgp	Matrix Gla protein	NM_008597	4.55	5.50E-06
Tnfrsf11b	TNF receptor superfamily member 11b	NM_008764	4.17	1.45E-05
Krt8	Keratin 8	NM_031170	3.70	5.90E-06
Vcam1	Vascular cell adhesion molecule 1	NM_011693	3.57	4.64E-05
Id4	Inhibitor of DNA binding 4	NM_031166	3.45	3.70E-06
Thbs2	Thrombospondin 2	NM_011581	3.45	1.31E-05
Pdgfr1	Platelet-derived growth factor receptor-like	NM_026840	3.03	6.40E-06
Ptrf	Caveolae associated 1	NM_008986	2.86	2.80E-06
Gadd45g	Growth arrest and DNA-damage-inducible 45 gamma	NM_011817	2.78	7.21E-05
Rab32	RAB32, member RAS oncogene family	NM_026405	2.70	8.90E-06
Lxn	Latexin	NM_016753	2.63	9.00E-07
Csrp2	Cysteine and glycine-rich protein 2	NM_007792	2.56	1.10E-06
Eno3	Enolase 3	NM_007933	2.56	3.00E-06
Sparc	Secreted acidic cysteine rich glycoprotein	NM_009242	2.56	6.02E-05
Id2	Inhibitor of DNA binding 2	NM_010496	2.56	1.15E-04
Nuak1	NUAK family, SNF1-like kinase, 1	NM_001004363	2.50	1.40E-06
Tmem86a	transmembrane protein 86A	NM_026436	2.44	3.50E-06
Dap	death-associated protein	NM_146057	2.33	4.40E-05
AA467197		NM_001004174	2.33	6.03E-05
Gpnmb	Glycoprotein (transmembrane) nmb	NM_053110	2.33	5.42E-04
AI467606		NM_178901	2.27	1.40E-06
Akr1c18	Aldo-keto reductase family 1, member C18	NM_134066	2.27	1.59E-04
Csnk	Casein kappa	NM_007786	-2.28	1.63E-04
Sox12	SRY (sex determining region Y)-box 12	NM_011438	-2.32	6.10E-06
2810003C17 Rik	Allograft inflammatory factor 1-like	NM_145144	-2.32	1.38E-05
Slpi	Secretory leukocyte peptidase inhibitor	NM_011414	-2.36	2.79E-04
Wfdc2	WAP four-disulfide core domain 2	NM_026323	-2.63	3.76E-05
1810015A11 Rik	YdjC homolog	NM_026940	-2.69	1.23E-05
Chchd10	Coiled-coil-helix-coiled-coil-helix domain containing 10	NM_175329	-2.74	3.09E-04
Bgn	Biglycan	NM_007542	-2.83	2.00E-07
Olfml2b	Olfactomedin-like 2B	NM_177068	-2.87	7.26E-05
LOC100048733		XM_001481081	-3.07	1.50E-06
Ak3	Adenylate kinase 3	NM_021299	-3.27	1.93E-05
4732462B05 Rik		AK028848	-4.13	2.70E-06



**Supplementary Table S3.** Top 40 genes differentially expressed in both D2A1-m1 and D2A1-m2 vs. D2A1 cells

Symbol	Gene name	Accession number	Average fold change
Arhgdib	Rho, GDP dissociation inhibitor beta	NM_007486	12.13
Mgp	Matrix Gla protein	NM_008597	10.63
Fgf7	Fibroblast Growth Factor 7	NM_008008	10.10
Casp1	Caspase 1	NM_009807	7.46
Lgals7	Galectin 7	NM_008496	7.25
Itgbl1	Integrin Subunit Beta Like 1	NM_145467	5.88
Tpm2	Tropomyosin 2, beta	NM_009416	4.97
Thbs2	Thrombospondin 2	NM_011581	4.93
Tnfrsf11b	TNF receptor superfamily member 11b	NM_008764	4.89
Id4	Inhibitor of DNA binding 4	NM_031166	4.62
Pdgfrl	Platelet-derived growth factor receptor-like	NM_026840	4.54
Akr1c18	Aldo-keto reductase family 1, member C18	NM_134066	3.58
Krt8	Keratin 8	NM_031170	3.58
Vcam1	Vascular cell adhesion molecule 1	NM_011693	3.40
AA467197		NM_001004174	3.20
Ptrf	Caveolae associated 1	NM_008986	3.03
Chst1	Carbohydrate (keratan sulfate Gal-6) sulfotransferase 1	NM_023850	3.00
Lxn	Latexin	NM_016753	2.78
Aqp1	Aquaporin 1	NM_007472	2.76
Idb4	Inhibitor of DNA binding 4	AK041164	2.59
Tmem86a	Transmembrane protein 86A	NM_026436	2.59
Gadd45g	Growth arrest and DNA-damage-inducible 45 gamma	NM_011817	2.49
Ank	Progressive ankylosis	NM_020332	2.45
AI467606		NM_178901	2.44
Dap	death-associated protein	NM_146057	2.44
Aqp5	Aquaporin 5	NM_009701	2.38
Axl	AXL receptor tyrosine kinase	NM_009465	2.27
Ecm1	Extracellular matrix protein 1	NM_007899	2.25
Gli2	GLI-Kruppel family member GLI2	NM_001081125	-2.31
Tuft1	Tuftelin 1	NM_011656	-2.37
Csnk	Casein kappa	NM_007786	-2.39
Cgn	Cingulin	XM_001001375	-2.41
Ogn	Osteoglycin	NM_008760	-2.67
LOC100048733		XM_001481081	-2.81
1810015A11Rik	YdjC homolog	NM_026940	-2.85
Bgn	Biglycan	NM_007542	-2.91
Ak3	Adenylate kinase 3	NM_021299	-3.07
Chchd10	Coiled-coil-helix-coiled-coil-helix domain containing 10	NM_175329	-3.13
Ptx3	Pentraxin related gene	NM_008987	-3.46
4732462B05Rik		AK028848	-4.13

**Supplementary Table S4. Top cellular and molecular functions identified by IPA**

	<i>p</i> -value	Activation z-score	# genes
<b>D2A1-m1 vs. D2A1</b>			
Cellular Movement	3.63E-03 - 5.69E-09		79
migration of cells*	5.69E-09	2.105	67
migration of breast cancer cell lines*	4.28E-05	2.179	14
Cell Death and Survival	3.49E-03 - 7.79E-08		101
cell survival*	2.83E-03	2.012	38
Cellular Assembly and Organisation	3.19E-03 - 6.74E-07		65
organization of cytoplasm*	6.74E-07	2.355	52
organization of cytoskeleton*	8.45E-06	2.567	46
Cellular Function and Maintenance	3.77E-03 - 6.74E-07		103
Cellular Development	3.50E-03 - 1.03E-06		92
<b>D2A1-m2 vs. D2A1</b>			
Cellular Movement	2.19E-03 - 1.54E-11		82
cell movement*	1.54E-11	2.414	79
migration of cells*	4.53E-11	2.602	72
Cell Death and Survival	1.73E-03 - 1.70E-08		105
cell death of connective tissue cells*	5.10E-04	2.113	21
cell survival*	8.36E-04	2.535	40
cell viability*	1.73E-03	2.604	37
Cellular Assembly and Organisation	2.04E-03 - 4.56E-08		76
Cellular Function and Maintenance	1.93E-03 - 4.56E-08		94
Cellular Development	2.22E-03 - 7.64E-08		102
<b>Common in D2A1-m1 and D2A1-m2 vs. D2A1</b>			
Cellular Movement	5.76E-03 - 7.79E-07		41
migration of cells*	7.49E-07	2.125	21
Cell Morphology	5.62E-03 - 7.49E-05		21
Cellular Assembly and Organisation	5.62E-03 - 7.49E-05		32
Small Molecule Biochemistry	5.62E-03 - 9.36E-05		16
Cell-To-Cell Signaling and Interaction	5.62E-03 - 1.05E-04		24
binding of connective tissue cells*	1.16E-03	2.394	6
adhesion of connective tissue cells*	4.13E-03	2.198	5

\*Predicted activation, z-score >2 or inactivation, z-score <-2

**Supplementary Table S5. Top upstream regulators identified by IPA**

	<i>p</i> -value of overlap	Activation z-score
<b>D2A1-m1 vs. D2A1</b>		
TP53	7.17E-13	1.962
TGFB1	2.44E-12	0.532
HRAS	8.46E-11	1.551
CTNNB1	1.20E-10	1.281
ERBB2	3.15E-10	0.665
KRAS	9.12E-10	0.561
IKBKB	2.01E-08	1.227
<b>HTT*</b>	<b>2.25E-08</b>	<b>2.128</b>
MYC	2.28E-08	-0.576
LH	5.19E-08	1.567

**D2A1-m2 vs. D2A1**

<b>TGFB1*</b>	<b>8.58E-19</b>	<b>2.651</b>
TP53	2.95E-12	1.681
MYC	6.61E-11	0.869
TNF	3.91E-09	1.962
TGFBR2	4.28E-09	1.083
<b>SMARCA4*</b>	<b>9.13E-09</b>	<b>2.159</b>
CTNNB1	7.10E-08	1.610
IKBKB	8.30E-08	-0.077
HRAS	8.39E-08	0.597
KRAS	2.52E-07	0.077

**Common in D2A1-m1 and D2A1-m2 vs. D2A1**

TGFB1	1.50E-11	1.129
KRAS	1.87E-08	0.218
IKBKB	3.43E-08	0.705
CTNNB1	5.50E-07	1.370
NFKBIA	1.02E-06	-1.021
MYC	2.58E-06	0.036
SMO	4.62E-06	
HRAS	5.24E-06	0.186
SMARCA4	7.66E-06	1.718
TP53	1.06E-05	1.176

\*Predicted activation, z-score >2 or inactivation, z-score <-2